PERGAMON

International Journal of Solids and Structures 38 (2001) 4017–4043

INTERNATIONAL JOURNAL OF SOLIDS and STRUCTURES

www.elsevier.com/locate/ijsolstr

A multilevel analysis of solid laminated composite beams

Omri Rand *

Faculty of Aerospace Engineering, Technion – Israel Institute of Technology, Haifa 32000, Israel

Received 19 June 1999

Abstract

The derivation and implementation of a multilevel analysis methodology for solid laminated composite beams is presented. The methodology is based on a hierarchy of solution levels that enable the prediction of a wide spectrum of physical phenomena including gross quantities such as the beam bending, extension, and twist components, and local phenomena such as the in-plane warping, interlaminar stresses and delamination effects. Three main solution levels are proposed. In the first level (level I), only the cross-sectional displacements, elastic twist and out-of-plane warping are included. The second level (level II) includes the prediction of the in-plane warping. The third level (level III) accounts for the interlaminar conditions and provides continuous stresses across interface lines in the case of bonded laminae, or alternatively, satisfy the appropriate boundary conditions in regions where delamination occurs. By providing a complete three-dimensional solution, the above separation of the problem into a set of solution levels provides an efficient solution methodology and supplies a better insight into the phenomena associated with the deformation of realistic orthotropic beams.

Keywords: Composite beams; Solid beams; Multilevel analysis

1. Introduction

The increasing use of composite beams is a well-known trend in many engineering applications. Besides their improved fatigue characteristics and high strength to weight ratio, composite materials offer many additional design degrees of freedom and provide solutions for applications which were previously based on a compromise between many different and contradicting demands. One of the profound features of composite beams is the ability to introduce passive couplings into their structural mechanisms. It may be shown that a proper layup design may induce couplings between the main elastic deformation components of composite beams, namely, the transverse displacements, the axial displacement, and the twist (Chandra et al., 1990; Rand, 1994). Elastic couplings may be exploited for ''passive'' augmentation of both the static and the dynamic characteristics of composite beams. Improvements of the vibratory characteristics and augmentation of the stability margins of helicopter blades is a typical example for potential applications that may benefit from elastic couplings (Berdichevsky et al., 1992; Smith and Chopra, 1993; Yamane and Friedmann, 1993; Tracy and Chopra, 1995; Bull, 1995; Rand and Barkai, 1996).

* Tel.: +972-4-829-3487; fax: +972-4-823-1848.
E-mail address: aeromri@ae560.technion.ac.il (O. Rand).

0020-7683/01/$ - see front matter
PII: S0020-7683(00)00256-0

The analysis of composite beams is by far more complicated than a similar analysis of isotropic beams. The elastic couplings in orthotropic laminae emerge from the material level that exhibits coupling between normal stress and shear strain and between shear stress and normal strain. In practice, the analysis of composite beams has been originated from the classical isotropic plates solution methodologies by modifying the material constitutive relations (Ochoa and Reddy, 1992; Kapania and Raciti, 1989). The resulting models were originally suitable for thin plates and in many cases, the term "composite beam" still refers to a slender thin beam ("plate-beam" models) where mainly the beam bending in its "soft" direction is under discussion.

It may be shown that unlike analyses of isotropic beams, adequate prediction of the behavior and in particular the elastic couplings in composite beams must be based on a detailed modeling of the distortion of the cross-sections (i.e. the planes perpendicular to the beam axis before deformation) which is generally termed *shear deformation*. The most important shear deformation component is the axial one and it will be referred to as the *out-of-plane warping* in what follows. The other warping components that modify the cross-sectional shape are referred to as the *in-plane warping*. Hence, due to the important role played by the warping in the overall behavior of the beams, and in particular in the determination of the coupling mechanisms, the earlier models were improved by higher-order shear deformation theories (Noor and Burton, 1989; Kapania and Raciti, 1989; Nosier and Reddy, 1992; Chandrashekhara and Bangera, 1992; Maiti and Sinha, 1994), whereas Wang and Choi (1982) represents studies that were aimed towards local phenomena such as the boundary effects in laminated composites. Most of the above mentioned analyses are focused on relatively simple "background loading" of the composite laminae such as uniform axial strain or prescribed load distribution over one of the cross-sectional edges.

Robbins and Reddy (1993) presents an exceptional and unique model that has been developed for thick laminae based on a separate displacement field for each lamina. When applied to thick composites, the analysis is capable of efficiently determining the interlaminar stresses and local effects. The formulation provides displacement continuity across interlaminar interfaces but allows for discontinuous strain components (i.e. discontinuous displacement derivatives). This model has a special relevancy to the solution methodology presented in this paper as will be clarified later on.

As far as the gross behavior of a composite beam is concerned, an important category of solution schemes which is based on an equivalent single layer analysis should be noted. In this category, the displacement derivatives (i.e. the strains) are continuous across the entire thickness and therefore the transverse stress components are discontinuous across lamina interfaces. Such an assumption may be valid for predicting global characteristics of thick laminae but is not adequate for predicting interlaminar phenomena. More details may be found in the works of Reddy (1989, 1990).

Since the warping is a local characteristic, detailed numerical models for realistic beams that are capable of dealing with both large global deformation and all warping components, are typically based on enormous number of degrees of freedom. The works of Giavotto et al. (1983) and Stemple and Lee (1989) are representative numerical schemes that are based on relatively large number of degrees of freedom, which include the necessary warping features, and yet contain some simplifying assumptions that ease their implementation. In general, such models do not always supply enough insight into the structural mechanisms and impose limitations on their usage in optimizations studies where many evaluations of the structural analysis are required.

The present analysis is based on a multilevel solution procedure. The analysis employs a series of solutions which are properly interconnected. Each solution is focused on a different level of the structural response. The level hierarchy emerges from the fact that all "upwards" data (from a lower level to an upper level) is of primary importance for the upper level solution, while all "downwards" data (from an upper level to a lower level) is of a secondary (or lower) importance to the lower level. As a results, all downwards information may be viewed as a "small correction" for the lower level which results in excellent convergence properties of the entire procedure. The present analysis deals with three levels of solutions, but additional levels are possible.

The multilevel analysis presented in this paper is based on a *graduate inclusion of physical effects* according to their overall importance and the changes they might induce on other physical phenomena. When dealing with composite beams, the global bending, twist and extension are the primary group of parameters. Then, the cross-sectional distortion (or the in-plane warping) constitute a set of additional deformation parameters that should be determined, and subsequently, the interlaminar effects have to be considered. As mentioned above, solutions of lower levels influence dramatically solutions of higher levels but not vice versa. Yet, all levels are consistently and fully coupled, hence, once the overall multilevel process is converged – all equations of equilibrium and boundary conditions are satisfied simultaneously and therefore constitute a unique three-dimensional solution of this linear problem. Practically, this methodology enables focusing and studying the associated phenomena at each level while ignoring irrelevant data from other levels. In addition to its efficiency, this feature enables a clear insight into the phenomena associated with each solution level.

To clarify the contribution of the proposed methodology, it should be mentioned that the literature contains *numerical methodologies* that are titled as "multiscale", "global–local" and "hierarchical" approaches (Fish and Markolefas, 1994; Belsky et al., 1995; Mitchell and Reddy, 1998). The above analyses are based on numerical techniques, and usually on finite-element based solution schemes, that allow analyses with various levels of meshing refinement at various locations over the structure. Subsequently, these solutions are based on detailed meshing of areas of interest which enables to capture fine local effects that are of smaller scale and could not be captured by the lower level (coarse) analysis although all physical phenomena were modeled in both levels. It may be stated that the main focus of the above analyses is the tailoring of the different numerical meshing used in different levels. The reader is also referred to the model reported by Savoia et al. (1993a,b), wherein iterative variational approach has been applied to a laminated beam model which was focused on the boundary layer analysis. In contrast with this class of methods, and although one may adopt some numerical techniques in order to implement the present analysis as well, the essence of the present approach is *independent of any numerical aspect and level of discretization* while as stated earlier, the levels differ by their content of physical phenomena. In fact, the present approach is also demonstrated by an *analytic* example in what follows. To make this point even clearer, it should be mentioned that the multilevel strategy offered in this paper is not a "grid correction" but rather hierarchy of physical phenomena, while higher levels phenomena are determined in the background posed by the lower level phenomena (and subsequently hardly influence this background state).

Additional clarification is required in order to distinguish the present analysis from the common analysis of composite laminates. The term "beam" used in this paper stands for the case of a slender structure which is subjected to a generic distribution of loads and both global deformation (i.e. bending in two perpendicular transverse directions, twist and extension) and local deformation (three warping components and a detailed interlaminar analysis) are of interest. In contrast with the analysis of laminates, the beam cross-sections may be very thick (such as a square cross-section) and both global (i.e. end effects) and local (i.e. free-traction outer surface) boundary conditions are accounted for while their mutual influences are consistently included in the analysis without any "high-order shear deformation" assumptions. Thus, overall, the proposed analysis offers a three-dimensional modeling of a realistic solid composite beam that accounts for all levels of physical phenomena and may handle a generic distribution of loads.

2. Problem statement

An illustrative deformed composite beam of solid cross-section is shown in Fig. 1a. Before deformation, the beam is straight and untwisted while the coordinates y and z define the cross-sectional planes and the x axis passes through the cross-sectional centroid. The beam is constructed out of orthotropic laminae which are parallel to the x–y plane as shown in Fig. 1b.

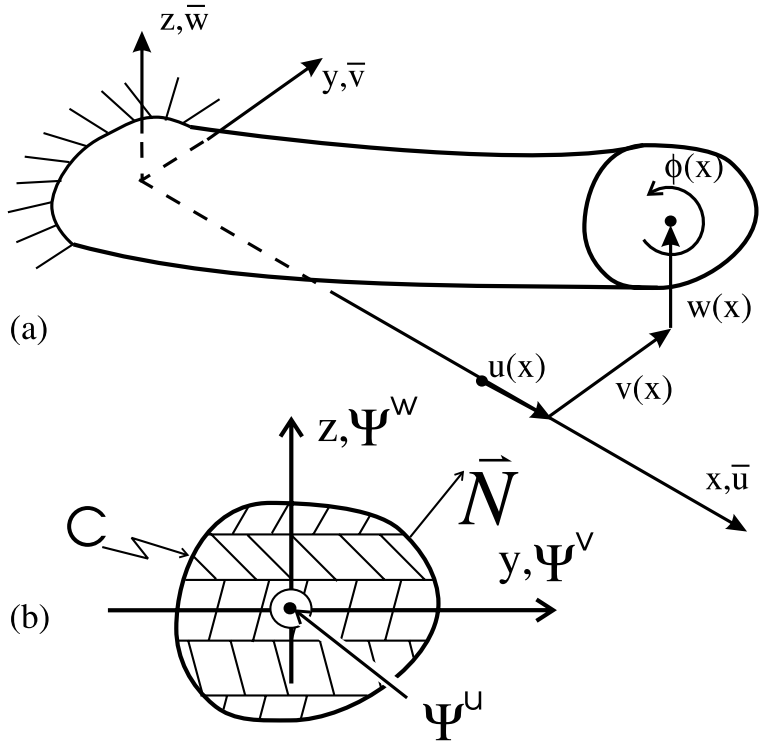

Fig. 1. Description of the deformation components of an orthotropic laminated beam: (a) the four cross-sectional components u, v, w and ϕ (functions of x only) and (b) the three warping components Ψ^u, Ψ^v and Ψ^w (three-dimensional functions).

It is convenient to describe the elastic deformation, $\bar{u}$, $\bar{v}$ and $\bar{w}$ in the x, y and z directions, respectively, as

$$\bar{u} = u - yv_{,x} - zw_{,x} + \Psi^u, \tag{1a}$$

$$\bar{v} = v - z\phi + \Psi^v, \tag{1b}$$

$$\bar{w} = w + y\phi + \Psi^w, \tag{1c}$$

where $u = u(x)$, $v = v(x)$, $w = w(x)$ are the displacement components in the x, y and z directions, respectively, and $\phi = \phi(x)$ is the cross-sectional twist angle. $\Psi^u(x,y,z)$ is the out-of-plane warping (i.e. in the x direction), while $\Psi^v(x,y,z)$ and $\Psi^w(x,y,z)$ are the components of the in-plane warping in the y and z directions, respectively. These three generic warping functions are superimposed upon the above mentioned u, v, w and ϕ deformation components and are assumed to be of zero average value over the cross-sectional area (i.e. $\int\int \Psi^u \mathrm{d}A = \int\int \Psi^v \mathrm{d}A = \int\int \Psi^w \mathrm{d}A = 0$). Additional boundary conditions for these warping functions will be dealt with in what follows. In this linear case, no distinction is made between the deformed and the undeformed directions and the order of superposition of the deformation components is immaterial.

The above separation of the displacements into cross-sectional components (u, v, w and ϕ) and local warping components (Ψ^u, Ψ^v and Ψ^w) is convenient due to the fact that the beam slenderness induces cross-sectional displacements which are many orders of magnitudes higher than the warping components. Yet, these warping deformation components play a key role in the involved physical phenomena.

Examination of the general constitutive relations for unbalanced orthotropic lamina which is parallel to the x–y plane and the principal axis of which does not coincide with the x direction, shows that the stress–strain relations may be written as

$$\{\sigma\} = [C]\{\varepsilon\}, \tag{2}$$

where the stiffness matrix $[C]$ is given by

$$[C] = \begin{bmatrix} C_{11} & C_{12} & C_{13} & 0 & 0 & C_{16} \\ C_{12} & C_{22} & C_{23} & 0 & 0 & C_{26} \\ C_{13} & C_{23} & C_{33} & 0 & 0 & C_{36} \\ 0 & 0 & 0 & C_{44} & C_{45} & 0 \\ 0 & 0 & 0 & C_{45} & C_{55} & 0 \\ C_{16} & C_{26} & C_{36} & 0 & 0 & C_{66} \end{bmatrix}. \tag{3}$$

The elastic moduli C_{ij} are functions of the material properties and the ply angle relative to the x axis (Ochoa and Reddy, 1992), and $\{\sigma\}$ and $\{\varepsilon\}$ are the stress and strain vectors, respectively, namely,

$$\{\sigma\} = \langle \sigma_{xx}, \sigma_{yy}, \sigma_{zz}, \tau_{yz}, \tau_{xz}, \tau_{xy} \rangle, \tag{4}$$

$$\{\varepsilon\} = \langle \varepsilon_{xx}, \varepsilon_{yy}, \varepsilon_{zz}, \gamma_{yz}, \gamma_{xz}, \gamma_{xy} \rangle. \tag{5}$$

The beam undergoes a distribution of loads (forces and moments) in the x, y and z directions, in addition to tip loads (i.e. tip forces and moments). Boundary conditions may be classified into two categories. The first category includes the "beam" boundary conditions at both ends. In the present analysis, a "clamped-free" beam will be under discussion (Fig. 1a), and therefore, geometrical boundary conditions are imposed at the root while natural boundary conditions are imposed at the free tip. The second category includes the traction-free surface of the beam which supplies boundary conditions to all warping components. Additional details will be discussed later on.

3. Definition of solution levels

At this stage, the problem will be divided into three solution levels while as stated before, each level is responsible for the modeling of a different physical phenomenon. Fig. 2 describes the solution levels and their mutual influences. The first (lowest) level is denoted "level I" and includes the displacements $u(x)$, $v(x)$, $w(x)$ and $\phi(x)$ and the out-of-plane warping $\Psi^u(x,y,z)$. This analysis level ignores the in-plane warping and any of the interlaminar effects. Subsequently, a (higher) "level II" solution is aimed towards the determination the in-plane warping components, namely, the components $\Psi^v(x,y,z)$ and $\Psi^w(x,y,z)$. Further on, the (highest) "level III" solution is carried out to refine the solution by adjusting the interlaminar stresses along the interlaminar lines in the case of bonded laminae, or by refining the solution for local delamination effects. Possible further solution refinement which is beyond the scope of the present effort and may be titled as "level IV" solution, is the determination of edge delamination stress singularities (Chen and Huang, 1997) which may provide a prediction of delamination propagation characteristics.

All of the above solutions levels are interconnected (Fig. 2). As already indicated, the level hierarchy emerges from the fact that all "upwards" data (from a lower level to an upper level) is of primary importance for the upper level solution, while all "downwards" data (from an upper level to a lower level) is of a secondary (or lower) importance for the lower level. In other words, all constrains and effects produced by higher levels are feeded downwards and affect the lower level solutions and vice versa.

The following sections contain a detailed description of each level analysis, and its interaction with other levels. In practice, the solution is initiated by level I (with no data from levels II and III), continues on to level II (with no data from level III), and then continues on to level III. These three solution levels are executed again while all downwards data is accounted for. The process is repeated until convergence is achieved. Due to the hierarchy described above, and the fact that all upwards data is of primary importance

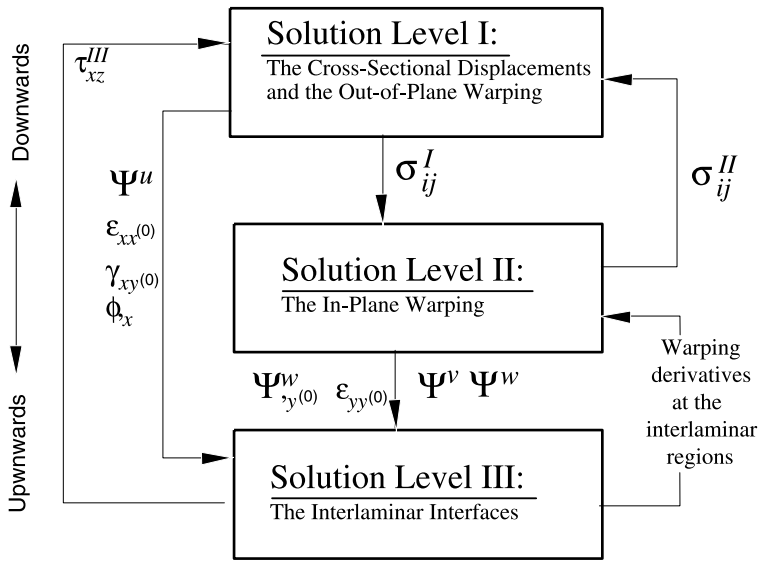

Fig. 2. Solution levels hierarchy and their mutual influences.

while downwards data may be considered as small correction, the above simple iterative process exhibits excellent convergence characteristics as will be demonstrated by the analytic example included in this paper. Included in this example are the analytic expressions for the iteration matrix of the process and an analytic evaluation of its spectral radius.

As already indicated, the above methodology enables the examination of the solution within each level while dealing with the most important physical parameters of this level while all the other parameters of the problem are treated as known background. This methodology may be executed in many and different analytic and/or numerical techniques. To demonstrate the capability of the present analysis, this paper includes (besides the analytic examples for simple cases), finite-difference based numerical schemes for generic cases and geometries.

3.1. Level I: the cross-sectional displacements and the out-of-plane warping

Level I solution includes the cross-sectional displacements $u = u(x)$, $v = v(x)$, $w = w(x)$ and $\phi = \phi(x)$ and the out-of-plane warping $\Psi^u(x,y,z)$. Thus, in this level, the in-plane warping components, $\Psi^v(x,y,z)$ and $\Psi^w(x,y,z)$, and the interlaminar phenomena are ignored, and their effect is accounted for by the data obtained from solutions levels II and III in terms of the stress distributions $\sigma_{xx}^{\mathrm{II}}$, τ_{xz}^{II}, τ_{xy}^{II} and τ_{xz}^{III} (Fig. 2).

Thus, within this level, only the following three components of strain are accounted for

$$\epsilon_{xx} = u_{,x} - yv_{,xx} - zw_{,xx} + \Psi^u_{,x}, \tag{6a}$$

$$\gamma_{xz} = y\phi_{,x} + \Psi^u_{,z}, \tag{6b}$$

$$\gamma_{xy} = -z\phi_{,x} + \Psi^u_{,y}, \tag{6c}$$

where ϵ_{xx} is the normal strain, γ_{xz}, γ_{xy} are the shear strains, and $(\ )_{,\alpha}$ denote differentiation with respect to α $(\alpha = x,y,z)$.

Based on Eq. (2) and the above discussion, the stresses σ_{xx}, τ_{xz} and τ_{xy} in this level are written as

$$\begin{Bmatrix} \sigma_{xx} \\ \\ \tau_{xz} \\ \\ \tau_{xy} \end{Bmatrix} = \begin{bmatrix} C_{11} & 0 & C_{16} \\ 0 & C_{55} & 0 \\ C_{16} & 0 & C_{66} \end{bmatrix} \begin{Bmatrix} \varepsilon_{xx} \\ \gamma_{xz} \\ \gamma_{xy} \end{Bmatrix} + \begin{Bmatrix} \sigma_{xx}^{\mathrm{II}} \\ \tau_{xz}^{\mathrm{II}} + \tau_{xz}^{\mathrm{III}} \\ \tau_{xy}^{\mathrm{II}} \end{Bmatrix}. \tag{7}$$

For this level I solution, the global deformation of the beam is treated and therefore an integral form of the equations of equilibrium should be constructed. Subsequently, equilibrium is achieved by four integral equations and one differential equation. The integral equations are obtained by assuming that the beam is a slender structure, and thus, the exact way of the introducing the external load to each cross-section is immaterial (in other words, as far as the external loads are concerned, the beam is viewed as a "thin line"). Hence, all distributed loads along the beam are treated as body forces. This assumption leads to a uniform traction-free boundary condition over the entire outer surface of the beam as will be shown later on. For that purpose, the differential equations of equilibrium are first integrated in the following form:

$$\int\int_A \left(\sigma_{xx,x} + \underline{\tau_{xz,z}} + \underline{\tau_{xy,y}} + B_x\right) \mathrm{d}A = 0, \tag{8a}$$

$$\int\int_A \left(\underline{\sigma_{yy,y}} + \tau_{xy,x} + \underline{\tau_{yz,z}} + B_y\right) \mathrm{d}A = 0, \tag{8b}$$

$$\int\int_A \left(\underline{\sigma_{zz,z}} + \tau_{xz,x} + \underline{\tau_{yz,y}} + B_z\right) \mathrm{d}A = 0, \tag{8c}$$

$$\int\int_A \left(\underline{\sigma_{zz,z}} + \tau_{xz,x} + \underline{\underline{\tau_{yz,y}}} + B_z\right) y \mathrm{d}A - \int\int_A \left(\underline{\sigma_{yy,y}} + \tau_{xy,x} + \underline{\underline{\tau_{yz,z}}} + B_y\right) z \mathrm{d}A = 0, \tag{8d}$$

where A is the cross-sectional area and B_x, B_y, B_z are the body forces in the x, y, z directions, respectively. It may be shown that integrals over the cross-sectional area of the once underlined quantities vanish due to their vanishing at the (traction-free) contour. In addition, the net contribution of the twice underlined terms is zero. It should be noted that the above integrations are carried out only for the purposes of constructing the equations for the solution in level I. For other levels, the exact local differential equations are fulfilled.

The definition of the longitudinal derivatives of the cross-sectional resultant forces F_x, F_y, F_z (in the x, y, and z direction, respectively) and the moment resultant M_x (in the x direction) are given by

$$F_{x,x} \equiv -\int\int_A B_x \mathrm{d}A = \int\int_A \sigma_{xx,x} \, \mathrm{d}A, \tag{9a}$$

$$F_{y,x} \equiv -\int\int_A B_y \mathrm{d}A = \int\int_A \tau_{xy,x} \, \mathrm{d}A, \tag{9b}$$

$$F_{z,x} \equiv -\int\int_A B_z \mathrm{d}A = \int\int_A \tau_{xz,x} \, \mathrm{d}A, \tag{9c}$$

$$M_{x,x} \equiv -\int\int_A \left(yB_z - zB_y\right) \mathrm{d}A = \int\int_A \left(y\tau_{xz,x} - z\tau_{xy,x}\right) \mathrm{d}A. \tag{9d}$$

Using the natural boundary values at the tip, namely $F_x^{\mathrm{t}} = \int\int_{A^{\mathrm{t}}} \sigma_{xx}^{\mathrm{t}} \mathrm{d}A^{\mathrm{t}}$, $F_y^{\mathrm{t}} = \int\int_{A^{\mathrm{t}}} \tau_{xy}^{\mathrm{t}} \mathrm{d}A^{\mathrm{t}}$, $F_z^{\mathrm{t}} = \int\int_{A^{\mathrm{t}}} \tau_{xz}^{\mathrm{t}} \mathrm{d}A^{\mathrm{t}}$ and $M_x^{\mathrm{t}} = \int\int_{A^{\mathrm{t}}} \left(y\tau_{xz} - z\tau_{xy}\right) \mathrm{d}A^{\mathrm{t}}$, the above four integral equations become (see also Eq. (7))

$$F_x = \int\int_A \left(\varepsilon_{xx}C_{11} + \gamma_{xy}C_{16}\right)\mathrm{d}A + \int\int_A \left(\sigma_{xx}^{\mathrm{II}}\right)\mathrm{d}A, \tag{10a}$$

$$F_y = \int\int_A \left(\varepsilon_{xx}C_{16} + \gamma_{xy}C_{66}\right)\mathrm{d}A + \int\int_A \left(\tau_{xy}^{\mathrm{II}}\right)\mathrm{d}A, \tag{10b}$$

$$F_z = \int\int_A \left(\gamma_{xz}C_{55}\right)\mathrm{d}A + \int\int_A \left(\tau_{xz}^{\mathrm{II}} + \tau_{xz}^{\mathrm{III}}\right)\mathrm{d}A, \tag{10c}$$

$$M_x = \int\int_A \left[y\left(\gamma_{xz}C_{55}\right) - z\left(\varepsilon_{xx}C_{16} + \gamma_{xy}C_{66}\right)\right]\mathrm{d}A + \int\int_A \left[y\left(\tau_{xz}^{\mathrm{II}} + \tau_{xz}^{\mathrm{III}}\right) - z\left(\tau_{xy}^{\mathrm{II}}\right)\right]\mathrm{d}A. \tag{10d}$$

The above equations are the integral equations for the cross-sectional unknowns $u = u(x)$, $v = v(x)$, $w = w(x)$ and $\phi = \phi(x)$. In addition a differential equation of equilibrium is required for the out-of-plane warping $\Psi^u(x,y,z)$ which is a local function. For that purpose, the differential equilibrium equation in x direction is explicitly used, namely,

$$\sigma_{xx,x} + \tau_{xy,y} + \tau_{xz,z} + B_x = 0. \tag{11}$$

Note that the integral equation in the x direction (Eq. (10a)) yields the determination of u while the differential equation supplies the out-of-plane warping $\Psi^u(x,y,z)$ which is a local function of zero average value. Hence, although both u and Ψ^u are deformation components in the x direction, they represent different ingredients.

There are eight boundary conditions for the cross-sectional displacements $u(x)$, $v(x)$, $w(x)$ and $\phi(x)$ at the blade root and tip, and a "contour" boundary condition for the warping function, Ψ^u, that should be satisfied over the entire contour of each cross-section. The geometric boundary conditions at the root for a clamped beam are

$$u = v = v_{,x} = w = w_{,x} = \phi = 0. \tag{12}$$

The natural boundary conditions at the blade tip are based on equating the transverse moments, M_y^{t} and M_z^{t}, to those obtained by integration of the stresses over the tip cross-sectional area, A^{t}:

$$M_y^{\mathrm{t}} = \int\int_{A^{\mathrm{t}}} \left[z\left(\varepsilon_{yy}C_{12} + \varepsilon_{zz}C_{13}\right)\right]\mathrm{d}A^{\mathrm{t}} + \int\int_{A^{\mathrm{t}}} \left[z\left(\sigma_{xx}^{\mathrm{II}}\right)\right]\mathrm{d}A^{\mathrm{t}}, \tag{13a}$$

$$M_z^{\mathrm{t}} = -\int\int_{A^{\mathrm{t}}} \left[y\left(\varepsilon_{yy}C_{12} + \varepsilon_{zz}C_{13}\right)\right]\mathrm{d}A^{\mathrm{t}} - \int\int_{A^{\mathrm{t}}} \left[y\left(\sigma_{xx}^{\mathrm{II}}\right)\right]\mathrm{d}A^{\mathrm{t}}. \tag{13b}$$

The contour boundary condition is based on the requirement of traction-free outer surface which may be expressed as (see also Fig. 1b)

$$\tau_{xz}\cos(\vec{N}, z) + \tau_{yz}\cos(\vec{N}, y) = 0 \quad \text{on } C, \tag{14}$$

where $\vec{N}$ is the local normal to the contour (Fig. 1b).

For level II solution, the following stress components are transferred (except for σ_{xx}^{I} which is provided below only for the sake of completeness), see also Eq. (2):

$$\begin{Bmatrix} \sigma_{xx}^{\mathrm{I}} \\ \tau_{xz}^{\mathrm{I}} \\ \tau_{xy}^{\mathrm{I}} \end{Bmatrix} = \begin{bmatrix} C_{11} & 0 & C_{16} \\ 0 & C_{55} & 0 \\ C_{16} & 0 & C_{66} \end{bmatrix} \begin{Bmatrix} \varepsilon_{xx} \\ \gamma_{xz} \\ \gamma_{xy} \end{Bmatrix}, \tag{15}$$

$$\begin{Bmatrix} \sigma_{yy}^{\mathrm{I}} \\ \sigma_{zz}^{\mathrm{I}} \\ \tau_{yz}^{\mathrm{I}} \end{Bmatrix} = \begin{bmatrix} C_{12} & 0 & C_{26} \\ C_{13} & 0 & C_{36} \\ 0 & C_{45} & 0 \end{bmatrix} \begin{Bmatrix} \varepsilon_{xx} \\ \gamma_{xz} \\ \gamma_{xy} \end{Bmatrix}. \tag{16}$$

For level III solution, the following strains at the interface lines (indicated as [](0)) are provided: $\varepsilon_{xx}(0)$ and $\gamma_{xy}(0)$, in addition to the value of $\phi_{,x}$ and the distribution of Ψ^u.

The implementation of the above described solution level I for generic configurations will be described later on.

3.2. Level II: the in-plane warping

Level II solution deals with the in-plane warping and the associated strain components. These quantities are related by

$$\varepsilon_{yy} = \Psi^{v}_{,y}, \tag{17a}$$

$$\varepsilon_{zz} = \Psi^{w}_{,z}, \tag{17b}$$

$$\gamma_{yz} = \Psi^{v}_{,z} + \Psi^{w}_{,y}. \tag{17c}$$

The solution in this level ignores the interlaminar effects. However, once a solution in level III has been carried out, the warping derivatives $\Psi^{w}_{,z}$ and $\Psi^{v}_{,z}$ on both sides of the interface line (i.e. at the laminae boundary) obtained by that solution are enforced in level II. The solution in level II is driven by the stresses of Eqs. (15) and (16) that were produced in level I solution (except for σ^{I}_{xx}). Thus, the stress components σ_{yy}, σ_{zz} and τ_{yz} in this case become (see also Eq. (2))

$$\begin{Bmatrix} \sigma_{yy} \\ \sigma_{zz} \\ \tau_{yz} \end{Bmatrix} = \begin{bmatrix} C_{22} & C_{23} & 0 \\ C_{23} & C_{33} & 0 \\ 0 & 0 & C_{44} \end{bmatrix} \begin{Bmatrix} \varepsilon_{yy} \\ \varepsilon_{zz} \\ \gamma_{yz} \end{Bmatrix} + \begin{Bmatrix} \sigma^{\mathrm{I}}_{yy} \\ \sigma^{\mathrm{I}}_{zz} \\ \tau^{\mathrm{I}}_{yz} \end{Bmatrix}. \tag{18}$$

Equilibrium within this solution is maintained by the two differential equations in the y and z directions, namely,

$$\sigma_{yy,y} + \tau_{yz,z} + \tau^{\mathrm{I}}_{xy,x} + B_y = 0, \tag{19a}$$

$$\sigma_{zz,z} + \tau_{yz,y} + \tau^{\mathrm{I}}_{xz,x} + B_z = 0. \tag{19b}$$

Eqs. (19a) and (19b) may be expressed using the above mentioned warping derivatives which yields a set of equations for $\Psi^{v}_{,zz}$, $\Psi^{w}_{,zz}$, $\Psi^{v}_{,yz}$ and $\Psi^{w}_{,yz}$. During the integrations of these equations, the values of $\Psi^{v}_{,z}$ and $\Psi^{w}_{,z}$ on both sides of the interface line serve as boundary values for the domain occupied by each lamina. These boundary values are supplied by the solution in level III as will be clarified later on.

The associated boundary conditions for traction-free edges are (see also Fig. 1b):

$$\sigma_{zz}\cos(\vec{N}, z) + \tau_{yz}\cos(\vec{N}, y) = 0, \tag{20a}$$

$$\sigma_{yy}\cos(\vec{N}, y) + \tau_{yz}\cos(\vec{N}, z) = 0. \tag{20b}$$

For the solution in level I, the following stress components are determined (Eq. (2)):

$$\begin{Bmatrix} \sigma^{\mathrm{II}}_{xx} \\ \tau^{\mathrm{II}}_{xz} \\ \tau^{\mathrm{II}}_{xy} \end{Bmatrix} = \begin{bmatrix} C_{12} & C_{13} & 0 \\ 0 & 0 & C_{45} \\ C_{26} & C_{36} & 0 \end{bmatrix} \begin{Bmatrix} \varepsilon_{yy} \\ \varepsilon_{zz} \\ \gamma_{yz} \end{Bmatrix}. \tag{21}$$

The values of Ψ^v, and Ψ^w at the interface regions are transferred to level III for further use as will be explained in what follows. In addition, the following strains at the interface lines are provided: $\varepsilon_{yy}(0)$ and $\Psi^{w}_{,y}$.

The implementation of the equations and boundary conditions in this level for generic cross-sectional configurations will be described later on.

3.3. Level III: the interlaminar interfaces

The solution in level III handles the interface regions. The discussion will be divided into two parts: the case of bonded laminae and the case of delaminated region.

3.3.1. An interface between two bonded laminae

Fig. 3a presents an interface line between two bonded laminae. The following discussion will concentrate on a typical vertical line which is perpendicular to the interface line. The same discussion holds for the vertical edges lines as well. The purpose of the solution in level III is to determine the warping on the interface line that will assure continuous stresses in the contact surface between laminae. The warping shown in Fig. 3 represents any one of the components Ψ^u, Ψ^v or Ψ^w. In what follows, the superscripts $(\ )^u$ $(\ )^v$ $(\ )^w$ of the warping will be omitted in cases where the discussions applies for all components.

Thus, from the level I or II solutions, the warping distributions which do not include the interlaminar phenomena are known (denoted by a broken line in Fig. 3a). The role of the solution in level III is to modify these warping distributions in the interlaminar area so that the relevant stresses over the interface line will be continuous. For that purpose, the values of the warping at the interface point $\overline{\Psi}^u$, $\overline{\Psi}^v$, $\overline{\Psi}^w$ are defined as unknowns, and the following discussion will describe the determination of $\overline{\Psi}^u$, $\overline{\Psi}^v$, $\overline{\Psi}^w$ for each vertical lines. For the sake of clarity, the discussion will describe the construction of the three equations that have to be solved at each interface point, provided that the warping $\overline{\Psi}^u$, $\overline{\Psi}^v$ and $\overline{\Psi}^w$ are known there, rather then providing closed expressions for these warping values.

Thus, for each set of interlaminar warping values $\overline{\Psi}^u$, $\overline{\Psi}^v$, $\overline{\Psi}^w$, it is possible to determine the derivatives $\Psi_{,z(-0)}$ and $\Psi_{,z(+0)}$ (i.e. the derivatives of $\Psi_{,z}$ on both sides of the interface line) and to express the strain components that contain displacement derivatives with respect to z as (see Eqs. (6b), (17b) and (17c)):

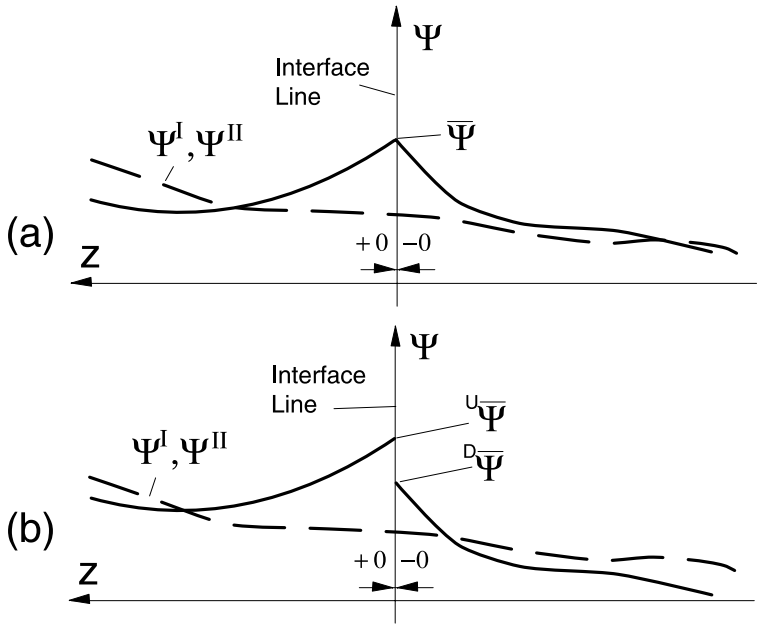

Fig. 3. A scheme of a warping distribution across an interlaminar line. The description holds for all warping components: (a) the case of bonded laminae and (b) the case of delaminated region.

$$\gamma_{xz(\pm 0)} = y_{(0)}\phi_{,x} + \Psi_{,z(\pm 0)}^{u}, \tag{22a}$$

$$\varepsilon_{zz(\pm 0)} = \Psi_{,z(\pm 0)}^{w}, \tag{22b}$$

$$\gamma_{yz(\pm 0)} = \Psi_{,y(0)}^{w} + \Psi_{,z(\pm 0)}^{v}, \tag{22c}$$

where "(0)" represents a value at the interface point. It should be noted that the value of $\Psi_{,y(0)}^{w}$ has been transferred to this level by level II solution and is continuous across the interface line. Similarly, $\phi_{,x}$ (which is constant over the entire cross-section) has been transferred from level I solution.

At this stage, the solution make use of $\varepsilon_{xx(0)}$ and $\gamma_{xy(0)}$ from level I and of $\varepsilon_{yy(0)}$ from level II which are all continuous across the interface line. By taking into account the different elastic moduli across the interface line, the stresses on both sides become

$$\sigma_{zz(\pm 0)} = C_{13(\pm 0)}\varepsilon_{xx(0)} + C_{23(\pm 0)}\varepsilon_{yy(0)} + C_{33(\pm 0)}\varepsilon_{zz(\pm 0)} + C_{36(\pm 0)}\gamma_{xy(0)}, \tag{23a}$$

$$\tau_{yz(\pm 0)} = C_{44(\pm 0)}\gamma_{yz(\pm 0)} + C_{45(\pm 0)}\gamma_{xz(\pm 0)}, \tag{23b}$$

$$\tau_{xz(\pm 0)} = C_{45(\pm 0)}\gamma_{yz(\pm 0)} + C_{55(\pm 0)}\gamma_{xz(\pm 0)}. \tag{23c}$$

Subsequently, the three linear equations for $\overline{\Psi}^{u}$, $\overline{\Psi}^{v}$ and $\overline{\Psi}^{w}$ that ensure equal stresses on both sides of the interface line are

$$\sigma_{zz(+0)} = \sigma_{zz(-0)}, \tag{24a}$$

$$\tau_{yz(+0)} = \tau_{yz(-0)}, \tag{24b}$$

$$\tau_{xz(+0)} = \tau_{xz(-0)}. \tag{24c}$$

This solution yields C^0 continuity of the displacement components through the interface line, while obviously, the strains on both sides of the interface point are different due to the discontinuous elastic moduli (see further discussion of this point in Robbins and Reddy (1993)). This characteristic of the present analysis will be demonstrated later on.

The outcome of this solution are the in-plane warping derivatives $\Psi_{,z}^{v}$ and $\Psi_{,z}^{w}$, on both sides of the interface lines which are transferred to level II solution. In addition, the values of $\Psi_{,z}^{u}$, $\Psi_{,zz}^{u}$ are used to construct the stress $\tau_{xz}^{\mathrm{III}} = C_{55}\Psi_{,z}^{u}$ used in level I and the values of $\tau_{xz,z}^{\mathrm{III}} = C_{55}\Psi_{,zz}^{u}$ which are required there.

3.3.2. A delaminated region

Similar to the case of bonded laminae, the discussion in this section will concentrate on a typical vertical line which is perpendicular to a delaminated interface line. The purpose of this version of level III solution is to determine the warping on both sides of the interface line that will assure traction-free edges at delaminated regions.

It should be noted that the equations presented in this section are valid only for the cases where the delaminated areas are known. As already mentioned, a more complete approach would be based on an inclusion of an additional level of solution which will be responsible for predicting the delaminated area by analyzing the stress singularities at the edge of the potential delaminated regions.

Fig. 3b illustrates the warping modification required at this stage. Again, from the level I and II solutions, the warping distribution which does not include the interlaminar phenomena is known (denoted by a broken line). The role of the solution in level III in this case is to determine the warping derivatives on both sides of the interface line so that the delaminated areas will be free of traction. However, in this case, the value of the warping at the lower edge of the upper lamina is not equal to the value of the same warping component at the upper edge of the lower lamina. Thus, six unknowns appear at each vertical line: ${}^{D}\overline{\Psi}^{u}$, ${}^{D}\overline{\Psi}^{v}$, ${}^{D}\overline{\Psi}^{w}$, ${}^{U}\overline{\Psi}^{u}$, ${}^{U}\overline{\Psi}^{v}$ and ${}^{U}\overline{\Psi}^{w}$ (Fig. 3b). Subsequently, the following discussions describes the determination of the above six warping unknowns for each vertical line that crosses an interlaminar surface.

Eqs. (22a)–(22c) are still applicable in this case by replacing $\overline{\Psi}$ with ${}^{D}\overline{\Psi}$ and ${}^{U}\overline{\Psi}$ for the lower and upper regions, respectively (i.e. for the cases of -0 and $+0$, respectively). Subsequently, Eqs. (23a)–(23c) are applicable as well. The condition for no contact between the laminae in the delaminated area yields the following six equations:

$$\sigma_{zz(+0)} = 0, \tag{25a}$$

$$\tau_{yz(+0)} = 0, \tag{25b}$$

$$\tau_{xz(+0)} = 0, \tag{25c}$$

$$\sigma_{zz(-0)} = 0, \tag{25d}$$

$$\tau_{yz(-0)} = 0, \tag{25e}$$

$$\tau_{xz(-0)} = 0. \tag{25f}$$

The solution of Eqs. (25a)–(25f) results in discontinuous values and derivatives of the warping on the interface line of a delaminated region. The determination of the warping derivatives for upper levels discussed in previous sections is valid for the present case as well.

4. The finite-difference scheme

As already indicated, the present approach is independent of any numerical methodology, and an analytic example for a relatively simple case will be described in what follows. Yet, for more complex configuration, a numerical approach is inevitable. To demonstrate the methodology offered in this paper for generic configurations, all of the above three solution levels have been implemented using a finite-difference scheme. It should be emphasized that finite-difference solutions have a special advantage in the present approach, since they enable a direct specification of the degrees of freedom and the governing equations (i.e. physical phenomena) that need to be included at each level. This separation is not trivial in other numerical methods such as the finite-element approach where a global formulation is inevitable.

4.1. General discretization aspects

In what follows, the discussion will be focused on the rectangular cross-section shown in Fig. 4a. For that purpose each cross-section is divided into $(N \times M)$ cells (M cells in the y direction and N cells in the z direction) which are not necessarily of equal size. A control point $(y_c(i,j), z_c(i,j))$ is defined at the middle of each cell. A warping value $\Psi^u(i,j)$, $\Psi^v(i,j)$, $\Psi^w(i,j)$ is defined at each control point. In addition, boundary control points are defined on all boundary edges and warping values $\Psi^{\alpha L}(i)$, $\Psi^{\alpha R}(i)$, $\Psi^{\alpha D}(j)$, $\Psi^{\alpha U}(j)$ $(\alpha = u, v, w)$ are assigned at these points. In addition, the beam is divided into N_x longitudinal segments as shown in Fig. 4b.

For the determination of displacement derivatives at a field point, a second-order polynomial approximation is used, which is equivalent to a "central derivative" when equally spaced data is under discussion. For example, to determine the $\partial \Psi^v_{(i,j)}/\partial y$ and $\partial^2 \Psi^v_{(i,j)}/\partial y^2$ derivatives at $(y_{c(j)}, z_{c(i)})$, the points $\Psi^v_{(i,j-1)}$, $\Psi^v_{(i,j)}$ and $\Psi^v_{(i,j+1)}$, and the corresponding locations $(y_{c(j-1)}, z_{c(i)})$, $(y_{c(j)}, z_{c(i)})$ and $(y_{c(j+1)}, z_{c(i)})$ are used to evaluate the polynomial approximation that fits these points, $\Psi^v \cong ay^2 + by + c$, while

$$a = \frac{\Delta_1(1,-1) - \frac{\Delta_1(0,-1)\delta_1(1,-1)}{\delta_1(0,-1)}}{\delta_2(1,-1) - \frac{\Delta_2(0,-1)\delta_1(k,l)}{\delta_1(k,l)}}, \tag{26a}$$

$$b = \frac{\Delta_1(0,-1) - a\Delta_2(0,-1)}{\delta_1(k,l)}, \tag{26b}$$

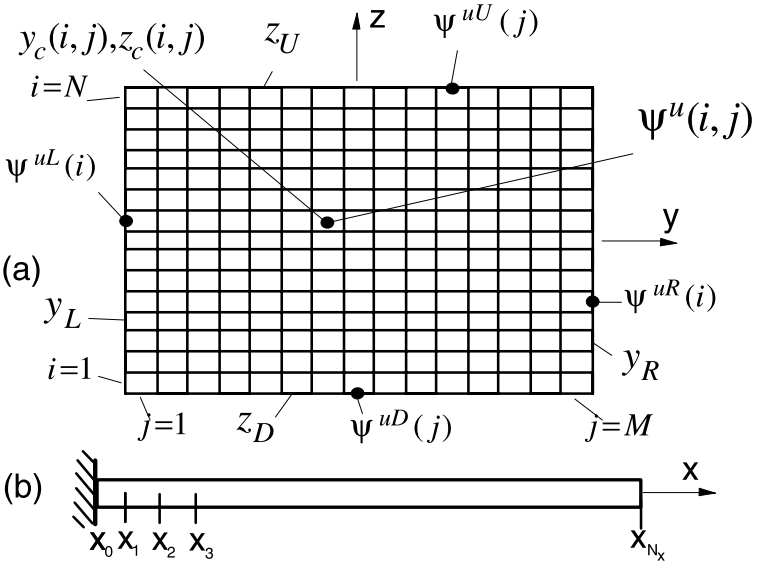

Fig. 4. A finite-difference discretization of a beam of a rectangular cross-section: (a) the cross-sectional discretization (only the Ψ^u warping component is shown) and (b) a spanwise discretization along the x axis.

where the following definitions are used:

$$\Delta_1(k,l) = \Psi^v_{(i,j+k)} - \Psi^v_{(i,j+l)}, \tag{27a}$$

$$\Delta_2(k,l) = \left(\Psi^v_{(i,j+k)}\right)^2 - \left(\Psi^v_{(i,j+l)}\right)^2, \tag{27b}$$

$$\delta_1(k,l) = y_{c(i,j+k)} - y_{c(i,j+l)}, \tag{27c}$$

$$\delta_2(k,l) = \left(y_{c(i,j+k)}\right)^2 - \left(y_{c(i,j+l)}\right)^2. \tag{27d}$$

Thus, the first and second derivatives at the $(y_{c(j)}, z_{c(i)})$ point become

$$\frac{\partial \Psi^v_{(i,j)}}{\partial y} = 2a y_{c(i,j)} + b, \tag{28a}$$

$$\frac{\partial^2 \Psi^v_{(i,j)}}{\partial y^2} = 2a. \tag{28b}$$

Identical technique is used for determining partial derivatives, and slightly modified procedure holds for boundary points.

4.1.1. Level I solution

With the aid of Eqs. (10a)–(10d) and (11) and the above described finite-difference scheme, it is possible to express the equations of equilibrium in terms of the displacements, and to construct a linear system of $(M \times N) + 2(N + M) + 4$ equations and unknowns for each cross-section which may be written as

$$[S]\{U\} = \{f\}, \tag{29}$$

where the unknown vector, $\{U\}$, is given by

$$\{U\} = \langle u_{,x}, v_{,xxx}, w_{,xxx}, \phi_{,x}, \Psi^u(1,1), \ldots, \Psi^u(N,M), \Psi^u_B(1), \ldots, \Psi^u_B(2(N+M)) \rangle^{\mathrm{T}}, \tag{30}$$

where Ψ^u_B consists of $\Psi^{uL}(i)$, $\Psi^{uR}(i)$, $\Psi^{uD}(j)$, $\Psi^{uU}(j)$. The local differential equation (Eq. (11)) supplies one equation per each cell (total of $M \times N$ equations), the contour boundary condition (Eq. (14)) supplies one equation per each boundary point (total of $2(M+N)$ equations), and the integral equilibrium equations (Eqs. (10a)–(10d)) supply additional four integral equations. Consequently, the loading vector $\{f\}$ consists of the external resultant loads and all other quantities that may not be expressed by the components of $\{U\}$. Generally, this vector may be written as

$$\{f\}^{\mathrm{T}} = \{f_1, f_2, f_3, f_4, f^1, f^2, f^3, \ldots, f^{MN+2(N+M)}\}, \tag{31}$$

where

$$f_1 = F_x + f_x(v_{,xx}, w_{,xx}, \Psi^u(i,j)_{,x}), \tag{32a}$$

$$f_2 = F_y + f_y(v_{,xx}, w_{,xx}, \Psi^u(i,j)_{,x}), \tag{32b}$$

$$f_3 = F_z, \tag{32c}$$

$$f_4 = M_x + m_x(v_{,xx}, w_{,xx}, \Psi^u(i,j)_{,x}), \tag{32d}$$

$$f^i = f^i(u_{,xx}, v_{,xx}, w_{,xx}, \Psi^u_{,x}, \Psi^u_{,xx}, \Psi^u_{,xy}, \Psi^u_B, \phi_{,xx}, B_x). \tag{32e}$$

The terms of the matrix $[S]$ and the vector $\{f\}$ are also explicit functions of the cross-sectional geometry and the elastic moduli distribution.

As shown above, the solution in level I includes longitudinal derivatives of both the cross-sectional displacements and the out-of-plane warping. Subsequently, this solution is based on internal iterations. The iterative scheme is initiated by some deformation assumption. Then, the resultant external loads at the discrete cross-sections along the beam (see $x_1 \ldots x_{N_x}$ in Fig. 4b) are evaluated. Subsequently, Eq. (29) is solved and the unknown vector, $\{U\}$, is obtained for each cross-section. The natural boundary conditions at the beam tip (Eqs. (13a) and (13b)) are then used to obtain the values of $v_{,xx}$, $w_{,xx}$ there. This is done by expressing the strain components of Eqs. (13a) and (13b) in terms of the displacements which yields two equations where the only unknowns are $v_{,xx}$, $w_{,xx}$. These values are then integrated along the beam and the distributions of $v_{,xx}(x)$ and $w_{,xx}(x)$ are obtained. With the aid of the geometric boundary conditions at the root (Eq. (12)), the distributions of u, $v_{,x}$, $w_{,x}$, v, w and ϕ along the beam are also determined. Using this new estimation of the deformation, the vector $\{f\}$ at each cross-section is updated (since it is a function of longitudinal derivatives of the unknowns, see Eqs. (32a)–(32e)), and the iterative process is repeated until convergence is achieved. Numerical study has shown that the above quasi-linear scheme exhibits excellent convergence characteristics.

It should be noted that the above internal iterations within level I emerge only from the specific numerical formulation described above which has been adopted for the sake of clarity. Different versions are possible including non-iterative solution procedures, and closed-form solutions for simple cases (Rand, 1994). In particular, the analysis in this level may be carried out by an FEM which accounts for the out-of-plane warping.

4.1.2. Level II solution

For the solution in level II, the unknowns are $\Psi^v_{(i,j)}$ $\Psi^w_{(i,j)}$ at each field point, $\Psi^{vL}_{(i)}$, $\Psi^{wL}_{(i)}$, $\Psi^{vR}_{(i)}$, $\Psi^{wR}_{(i)}$ on the vertical edges, and $\Psi^{vD}_{(j)}$, $\Psi^{wD}_{(j)}$ $\Psi^{vU}_{(j)}$, $\Psi^{wU}_{(j)}$ on the horizontal edges – see Fig. 4a. The field equations (Eqs. (19a) and (19b)) are applied at each cell point $(y_{c(j)}, z_{c(i)})$, and the boundary conditions (Eqs. (20a) and (20b)) are applied over the edges $(y_L, z_{c(i)})$ $(y_R, z_{c(i)})$ $(y_{c(j)}, z_D)$ $(y_{c(j)}, z_U)$.

Using the above described finite-difference scheme, the solution in this level may be put as a linear system of algebraic equations where the unknowns are the above warping values in the field and on the boundaries.

Thus, the system size is $2NM + 4(N + M)$. Note that the contributions of $\tau^{I}_{xy,x}$ and τ^{I}_{xz} that are evaluated by the solution in level I are the "forcing" terms in this system (Eqs. (19a) and (19b)). The solution in this level is a "one step" solution that includes no iterations.

As already discussed, the analysis in this level may be carried out by various other methodologies including the FEM which may be easily adapted to the cross-sectional domain.

4.1.3. Level III solution

Bonded laminae: A discrete description of the interface region is described in Fig. 5. Values related to the regions below and above the interface line are denoted by the left superscript "D" and "U", respectively. From level I and level II solutions, the values of ${}^{D}\Psi_{(1)}$, ${}^{D}\Psi_{(2)}$, ${}^{U}\Psi_{(1)}$ and ${}^{U}\Psi_{(2)}$ are known since these are control location of the finite-difference mesh. Subsequently, the unknown values of the warping at the interface point $\overline{\Psi}^{u}$, $\overline{\Psi}^{v}$ and $\overline{\Psi}^{w}$ are defined for each vertical line.

As a first step, for a given set of $\overline{\Psi}^{u}$, $\overline{\Psi}^{v}$ and $\overline{\Psi}^{w}$, the warping derivatives in the z direction just below the interface point (the point denoted -0 in Fig. 5) are determined based on $\overline{\Psi}$, ${}^{D}\Psi_{(1)}$ and ${}^{D}\Psi_{(2)}$. Similarly, the warping derivatives just above the interface point (the point denoted $+0$ in Fig. 5) are determined based on $\overline{\Psi}$, ${}^{U}\Psi_{(1)}$ and ${}^{U}\Psi_{(2)}$. For that purpose, Ψ is expanded in the "D" region as: $\Psi({}^{D}\zeta) \cong \overline{\Psi} + {}^{D}b\,{}^{D}\zeta + {}^{D}c\,{}^{D}\zeta^2$ where:

$$ {}^{D}b = \frac{\left({}^{D}\Psi_{(2)} - \overline{\Psi}\right){}^{D}\zeta^2_{(1)} - \left({}^{D}\Psi_{(1)} - \overline{\Psi}\right){}^{D}\zeta^2_{(2)}}{{}^{D}\zeta_{(2)}\,{}^{D}\zeta^2_{(1)} - {}^{D}\zeta_{(1)}\,{}^{D}\zeta^2_{(2)}}, \tag{33a} $$

$$ {}^{D}c = \frac{{}^{D}\Psi_{(1)} - \overline{\Psi}}{{}^{D}\zeta^2_{(1)}} - \frac{{}^{D}b}{{}^{D}\zeta_{(1)}}. \tag{33b} $$

Similarly, Ψ is expanded in the "U" region as: $\Psi({}^{D}\zeta) \cong \overline{\Psi} + {}^{D}b\,{}^{D}\zeta + {}^{D}c\,{}^{D}\zeta^2$ and the expressions for ${}^{U}b$ and ${}^{U}c$ are similar to those of Eqs. (33a) and (33b) (i.e. obtained by replacing the left superscript "D" by "U").

Thus, the first derivatives at both sides of the interface point are

$$ \Psi_{,z(-0)} = -{}^{D}b, \tag{34a} $$

$$ \Psi_{,z(+0)} = {}^{U}b. \tag{34b} $$

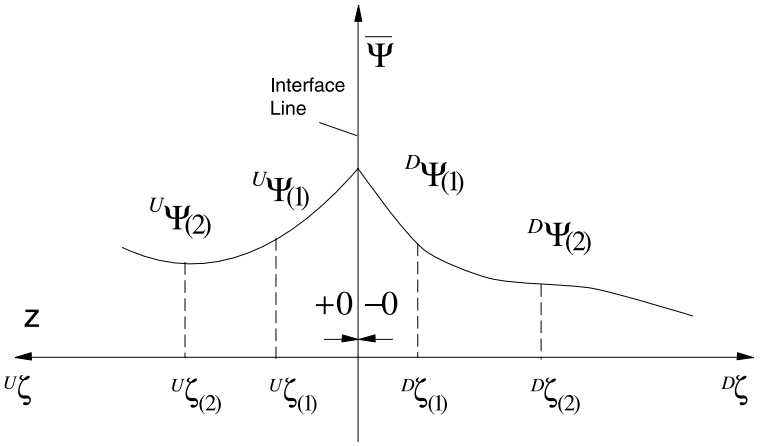

Fig. 5. Discretization of an interlaminar area in the case of bonded laminae (applies to each one of the warping components).

It is now possible to express the strain and the stress components described in Eqs. (22a)–(22c) and (23a)–(23c) and to apply system of three equations and unknowns of Eqs. (24a)–(24c) for each vertical line. The solution of this system yields the desired values of $\overline{\Psi}^{u}$, $\overline{\Psi}^{v}$ and $\overline{\Psi}^{w}$.

As shown in Fig. 2, level III solution results are fed "upwards" by means of the warping derivatives in the z direction on both sides of the interface line. Within the current finite-difference scheme, the following derivatives at the first control point are transferred to level II solution:

$$\Psi_{,z(^{D}\zeta_{(1)})} = -^{D}b - 2^{D}c^{D}\zeta_{(1)}, \tag{35a}$$

$$\Psi_{,z(^{U}\zeta_{(1)})} = {}^{U}b + 2^{U}c^{U}\zeta_{(1)}, \tag{35b}$$

$$\Psi_{,zz(^{D}\zeta_{(1)})} = 2^{D}c, \tag{35c}$$

$$\Psi_{,zz(^{U}\zeta_{(1)})} = 2^{U}c. \tag{35d}$$

In addition, the partial derivatives $\Psi_{,yz}$ at these points are evaluated by a finite-difference derivative of $\Psi_{,z}$ across adjacent vertical lines.

While the derivatives $\Psi_{,z}^{v}$, $\Psi_{,zz}^{v}$, $\Psi_{,z}^{w}$, $\Psi_{,zz}^{w}$, $\Psi_{,yz}^{v}$, $\Psi_{,yz}^{w}$ are fed upwards to solution level II, the derivatives $\Psi_{,z}^{u}$, $\Psi_{,zz}^{u}$, are fed upwards to solution level I. These values are used to construct τ_{xz}^{III} and $\tau_{xz,z}^{\mathrm{III}}$ at the $^{D}\zeta_{(1)}$, $^{U}\zeta_{(1)}$ locations.

A delaminated interface: Similar to the previous case, the values of $^{D}\Psi_{(1)}$, $^{D}\Psi_{(2)}$, $^{U}\Psi_{(1)}$ and $^{U}\Psi_{(2)}$ are known from the level I and level II solutions. However, at the interface point, the values of the warping at the lower edge of the upper lamina is not equal to the warping at the upper edge of the lower lamina. Thus, six unknowns appear in each vertical line: $^{D}\overline{\Psi}^{u}$, $^{D}\overline{\Psi}^{v}$, $^{D}\overline{\Psi}^{w}$, $^{U}\overline{\Psi}^{u}$, $^{U}\overline{\Psi}^{v}$ and $^{U}\overline{\Psi}^{w}$. Subsequently, six equations have to be solved for each vertical line.

Eqs. (33a) and (33b) are still applicable in this case by replacing $\overline{\Psi}$ with $^{D}\overline{\Psi}$ and $^{U}\overline{\Psi}$ for the upper and lower regions, respectively. Subsequently, Eqs. (34a) and (34b) are applicable as well. The condition of no contact between the laminae in the delaminated area turns to give the six equations given in Eqs. (25a)–(25f). The above Eqs. (35a)–(35d) hold for the present case as well and the derivatives values are fed to solution levels I and II as described in the previous section.

5. Consistency, stability and convergence

As already indicated, the proposed multilevel approach employs an iterative scheme where the solution levels are executed sequentially until convergence is achieved. When such a convergence is obtained for the *linear* problem under discussion, all equations of equilibrium and boundary conditions are satisfied simultaneously, and therefore the overall solution coincides with the three-dimensional solution. Therefore, when consistency, stability and convergence issues are raised, one should distinguish between two different classes of considerations. The first class should examine the corresponding characteristics of each solution level, while the second class should examine the consistency, stability and convergence of the system of levels that are proposed in this paper. Since each solution level may be executed using various solution methodologies, the characteristics of these solutions will not be discussed in the present context and it will be assumed that each one of these solution scheme is consistent and stable by its own. However, within the analytic example presented in what follows, an explicit evaluation of the iteration matrix of the overall multilevel process, $[\alpha]$, and its spectral radius, ρ_{α}, will be presented and discussed. Note again that this iteration matrix represents the stability and convergence of the overall iterations between solution levels and its explicit evaluation is possible only because of the analytic nature of the example. For generic cases, the iteration matrix has been obtained numerically.

6. Applications

The illustrative results presented in this section have been carried out for a typical Graphite/Epoxy laminae where $E_{11} = 130 \times 10^9$ N/m^2, $E_{22} = E_{33} = 10 \times 10^9$ N/m^2, $G_{12} = G_{13} = 6 \times 10^9$ N/m^2, $G_{23} = 3 \times 10^9$ N/m^2, $v_{12} = v_{13} = 0.3$ and $v_{23} = 0.5$.

6.1. Analytic example: the case of pure bending of homogeneous cross-sections

When dealing with the case where all laminae are identical and oriented at the same direction with respect to the x axis, a homogeneous cross-section is obtained (which may also be viewed as a "single lamina cross-section"). Therefore, this case reflects a "symmetric" layup that produces coupling between bending and twist. By activating solutions levels I and II only for this case (since there are no interface lines between different laminae), the above described formulations enables a closed-form analytic solution for the case where the beam undergoes a uniform bending moment, M_y. Such a solution provides a clear insight into the influence of the in-plane warping, demonstrates the multilevel analysis suggested in this paper including its convergence to the three-dimensional solution, and enables an explicit evaluation of the iteration matrix and its spectral radius. This analytic example also demonstrates the fact that the proposed methodology is independent of any numerical aspect of the problem.

Thus, the present analytic example deals with the case where the beam is assumed to undergo a uniform bending moment, M_y, which is applied at the tips by a linear axial stress distribution, namely $\sigma_{xx} = zM_y/I_{zz}$ where $I_{zz} = \int\int z^2 \mathrm{d}A$. In what follows, a three-dimensional exact solution of this problem will be first presented. Then, analytic solutions for both level I and level II are separately described, and subsequently, the proposed multilevel iterative methodology is demonstrated.

6.1.1. The three-dimensional exact solution

An exact solution for the above bending of unbalanced homogeneous orthotropic beam is presented in this section. The solution is quite general and applicable for *any* homogeneous simply connected cross-section. The derivation is based on some preliminary assumptions regarding parts of the displacement components. However, since these assumptions will be proved to produce an exact three-dimensional solution to the present problem, the uniqueness of such exact solution establishes the validity of all preliminary assumptions adopted throughout the derivation.

In general, the displacements, $\overline{u}$, $\overline{v}$ and $\overline{w}$ in the x, y and z directions, respectively, are given in Eqs. (1a)–(1c). To derive a closed form solution for the above described case, a solution of the following form is applied:

$$u(x) = 0, \tag{36a}$$

$$v(x) = 0, \tag{36b}$$

$$\Psi^u = Ayz, \tag{36c}$$

$$\Psi^v = Byz, \tag{36d}$$

$$\Psi^w = Cy^2 + Dz^2, \tag{36e}$$

where A, B, C and D are constants to be determined. In addition, $w_{,xx}$ and $\phi_{,x}$ are assumed to be constants along the beam. Using Eqs. (1a)–(1c) and (36a)–(36e), the strain components take the form:

$$\varepsilon_{xx} = -zw_{,xx}\,, \tag{37a}$$
$$\varepsilon_{yy} = Bz, \tag{37b}$$
$$\varepsilon_{zz} = 2Dz, \tag{37c}$$
$$\gamma_{yz} = 2Cy + By, \tag{37d}$$
$$\gamma_{xz} = \phi_{,x}\, y + Ay, \tag{37e}$$
$$\gamma_{xy} = -\phi_{,x}\, z + Az. \tag{37f}$$

The above expressions are substituting in the strain vector of Eq. (5), and the stress vector of Eq. (4) is determined with the aid of Eqs. (2) and (3). Thus, by setting $A = -\phi_{,x}$ and $C = -B/2$ in Eqs. (37d)–(37f), one obtains $\gamma_{xz} = \gamma_{yz} = 0$ and $\gamma_{xy} = -2z\phi_{,x}$, which with the aid of Eqs. (2)–(5) shows that $\tau_{yz} = \tau_{xz} = 0$. At this stage, it is possible to formulate the requirements for $\sigma_{yy} = \sigma_{zz} = \tau_{xy} = 0$ and $M_y = \int\int \sigma_{xx} z \mathrm{d}A$ as the following system of algebraic equations:

$$\begin{bmatrix} -C_{11} & -2C_{16} & C_{12} & 2C_{13} \\ -C_{12} & -2C_{26} & C_{22} & 2C_{23} \\ -C_{13} & -2C_{36} & C_{23} & 2C_{33} \\ -C_{16} & -2C_{66} & C_{26} & 2C_{36} \end{bmatrix} \begin{Bmatrix} w_{,xx} \\ \phi_{,x} \\ B \\ D \end{Bmatrix} = \begin{Bmatrix} M_y/I_{zz} \\ 0 \\ 0 \\ 0 \end{Bmatrix}. \tag{38}$$

The solution of Eq. (38) ensures that all stress components vanish, except for σ_{xx}. Consequently, it is evident that all differential equations of equilibrium and boundary conditions are satisfied *for any arbitrary cross-sectional geometry*. Subsequently, $w(x)$ and $\phi(x)$ may be integrated (for example, the case of $w(0) = w_{,x}(0) = \phi(0) = 0$ yields $w = w_{,xx}\, x^2/2$ and $\phi = \phi_x x$).

6.1.2. Solution by a multilevel approach

In what follows the present problem will be expressed in terms of solution levels and the multilevel approach will be demonstrated.

Level I: The solution in this level is based on the assumption (which will be proved to be exact later on) that the data from level II solution will be of the form $\sigma_{xx}^{\mathrm{II}} = a_1 z$, $\tau_{xy}^{\mathrm{II}} = a_2 z$, and $\tau_{xz}^{\mathrm{II}} = 0$, where a_1 and a_2 are constants, and clearly for the first iteration $a_1 = a_2 = 0$ will be used. In addition, u and v are set to zero, $w_{,xx}$ and $\phi_{,x}$ are assumed to be constants, and an out-of-plane warping of the following type is used:

$$\Psi^u = -\phi_{,x}\, yz. \tag{39}$$

Substituting the above initial assumptions in Eqs. (6a)–(6c) and (7) shows that

$$\sigma_{xx} = C_{11}(-zw_{,xx}) + C_{16}(-2z\phi_{,x}) + a_1 z, \tag{40a}$$
$$\tau_{xz} = 0, \tag{40b}$$
$$\tau_{xy} = C_{16}(-zw_{,xx}) + C_{66}(-2z\phi_{,x}) + a_2 z. \tag{40c}$$

It is now possible to determine $w_{,xx}$ and $\phi_{,x}$ from Eqs. (40a), (40b) by the requirements $\tau_{xy} = 0$ and $\sigma_{xx} = zM_y/I_{zz}$ which yield:

$$\begin{bmatrix} 2C_{66} & C_{16} \\ 2C_{16} & C_{11} \end{bmatrix} \begin{pmatrix} \phi_{,x} \\ w_{,xx} \end{pmatrix} = \begin{pmatrix} a_2 \\ a_1 - \frac{M_y}{I_{zz}} \end{pmatrix}. \tag{41}$$

The reader may verify that the above values for $w_{,xx}$, $\phi_{,x}$ and the expression for Ψ^u satisfy all equations of equilibrium (Eqs. (10a)–(10d) and (11)) and boundary conditions (Eqs. (12), (13a), (13b) and (14)) of level I. This concludes the solution in this level, while for the solution in level II, the following stress components are transferred (Eqs. (15) and (16)):

$$\begin{pmatrix} \tau^{\mathrm{I}}_{xy} \\ \sigma^{\mathrm{I}}_{yy} \\ \sigma^{\mathrm{I}}_{zz} \end{pmatrix} = -z \begin{bmatrix} 2C_{66} & C_{16} \\ 2C_{26} & C_{12} \\ 2C_{36} & C_{13} \end{bmatrix} \begin{pmatrix} \phi_{,x} \\ w_{,xx} \end{pmatrix} \tag{42}$$

while $\tau^{\mathrm{I}}_{xz} = \tau^{\mathrm{I}}_{yz} = 0$.

Level II: The solution in this level is based on the assumption that the in-plane warping components are of the form $\Psi^v = Byz$ and $\Psi^w = Cy^2 + Dz^2$ where B, C and D are constants. According to Eq. (18),

$$\sigma_{yy} = C_{22}Bz + 2C_{23}Dz + \sigma^{\mathrm{I}}_{yy}, \tag{43a}$$

$$\sigma_{zz} = C_{23}Bz + 2C_{33}Dz + \sigma^{\mathrm{I}}_{zz}, \tag{43b}$$

$$\tau_{yz} = C_{44}(B + 2C)y. \tag{43c}$$

The requirement for $\sigma_{yy} = \sigma_{zz} = \tau_{yz} = 0$ shows that $B + 2C = 0$ while B and D are obtained from:

$$\begin{bmatrix} C_{22} & C_{23} \\ C_{23} & C_{33} \end{bmatrix} \begin{pmatrix} B \\ 2D \end{pmatrix} = \begin{bmatrix} 2C_{26} & C_{12} \\ 2C_{36} & C_{13} \end{bmatrix} \begin{pmatrix} \phi_{,x} \\ w_{,xx} \end{pmatrix}. \tag{44}$$

The solution of the above system of equations ensures that both the differential equations, Eqs. (19a) and (19b), and the boundary conditions, Eqs. (20a) and (20b), are satisfied. This concludes the solution in level II while Eq. (21) is used to construct the stress components $\sigma^{\mathrm{II}}_{xx} = a_1 z$ and $\tau^{\mathrm{II}}_{xy} = a_2 z$ which are feeded back to level I, as

$$\begin{pmatrix} a_1 \\ a_2 \end{pmatrix} = \begin{bmatrix} C_{12} & C_{13} \\ C_{26} & C_{36} \end{bmatrix} \begin{pmatrix} B \\ 2D \end{pmatrix} \tag{45}$$

while as previously assumed $\tau^{\mathrm{II}}_{xz} = 0$. With these values the iterative process returns to level I, and the above steps are repeated until convergence is achieved.

6.1.3. The iterative multilevel process

Fig. 6a presents the nondimensional values of $-M_y/(C_{11}I_{zz}w_{,xx})$ and $-\phi_{,x}/w_{,xx}$ as functions of the iteration number, while Fig. 6b presents the variation of the nondimensional values of a_1 and a_2 as obtained by a sequential execution of the above solution levels for the material properties presented above and for a layup angle of 30°. As shown, convergence is achieved after six iterations and the reader may verify that the three-dimensional exact solution is reached. It is also evident that both the values of $w_{,xx}$ and $\phi_{,x}$ are modified by the in-plane warping, and that the values of iteration #1 correspond to the case where the in-plane warping is ignored.

6.1.4. Spectral radius

The above multilevel solution consists of two deformation parameters, $\phi_{,x}$ and $w_{,xx}$ that are transferred from level I to level II, and two deformation parameters, a_1 and a_2 that are fed back from level II to level I. Subsequently, an iteration matrix may be formulated for each one of these two sets of deformation parameters and a derivation of its spectral number may be carried out. To derive the iteration matrix for the a_1 and a_2 parameters, Eq. (41) is substituted into Eq. (44) and then Eq. (44) is substituted into Eq. (45). This enables to write

$$\begin{pmatrix} a_1 \\ a_2 \end{pmatrix}_{i+1} = [\alpha] \begin{pmatrix} a_1 \\ a_2 \end{pmatrix}_i + [\beta], \tag{46}$$

where the subscript i represents the iteration number. The iteration matrix, $[\alpha]$, is given by

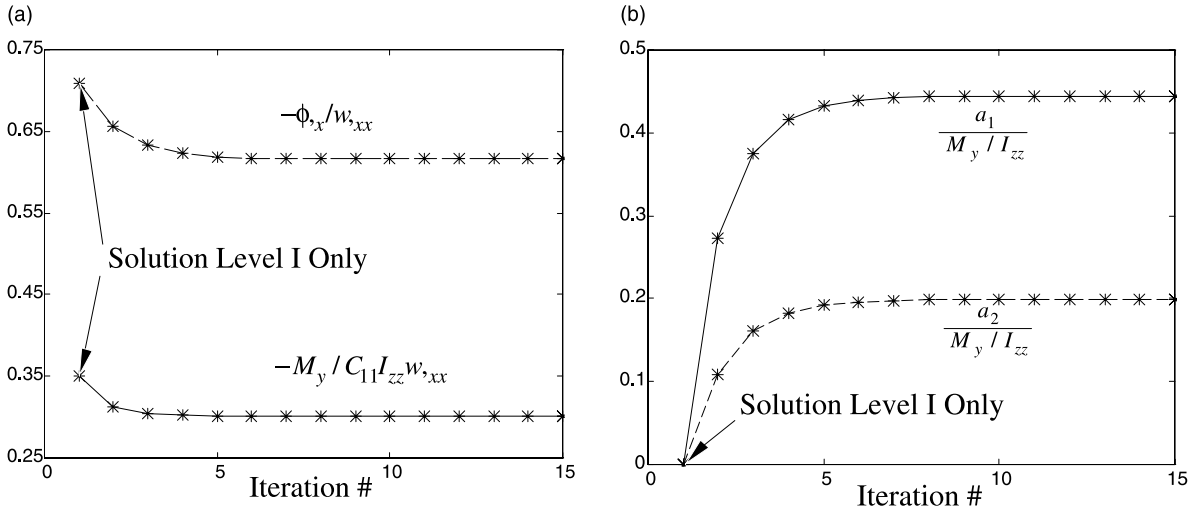

Fig. 6. (a) The values of $w_{,xx}$ and $\phi_{,x}$. (b) The values of a_1 and a_2 for homogeneous beam under pure bending moment, M_y, as obtained by the analytic solutions for levels I and II.

$$[\alpha] = \begin{bmatrix} C_{12} & C_{13} \\ C_{26} & C_{36} \end{bmatrix} \begin{bmatrix} C_{22} & C_{23} \\ C_{23} & C_{33} \end{bmatrix}^{-1} \begin{bmatrix} 2C_{26} & C_{12} \\ 2C_{36} & C_{13} \end{bmatrix} \begin{bmatrix} 2C_{16} & C_{11} \\ 2C_{66} & C_{16} \end{bmatrix}^{-1}, \tag{47a}$$

$$[\beta] = [\alpha] \begin{pmatrix} -M_y/I_{zz} \\ 0 \end{pmatrix}. \tag{47b}$$

Introducing the elastic moduli of the present example shows that the spectral radius of this example (defined as $\max_i |\lambda_i|$ where λ_i are the eigenvalues of $[\alpha]$) is $\rho_\alpha = 0.151$ (while the condition $\rho_\alpha \leqslant 1$ ensures stability and convergence of the scheme). As already stated, no general proof for generic configurations may be developed in the present context, since the proposed multilevel analysis is not confined to a specific solution methodology at each level (which may be based on high number of degrees of freedom). However, the above closed form solution and the determination of the spectral radius of the overall multilevel iteration process demonstrates the feasibility and applicability of the method to the present application of laminated composite beams.

To complete the present study of homogeneous cross-sections, Fig. 7a and b present the behavior of a clamped-free beam of homogeneous rectangular cross-section that undergoes a tip beamwise load. In the absence of a closed-form solution for this case, the solution has been obtained using the finite-difference scheme presented in this paper. Fig. 7a presents the "direct" deformation (i.e. beamwise displacement due to a beamwise load), while Fig. 7b presents the "induced" deformation (i.e. twist due to a beamwise load). As shown, the solution in level I by itself is not capable of adequately predicting the beamwise deflection for lamination angles above 20°, and the induced twist for angles above 40°. Similar trend has been observed in other loading modes.

6.2. Non-homogeneous cross-sections

6.2.1. An uncoupled beam

The discussion will now turn to the case of non-homogeneous cross-sections. As a first case, a symmetric and balanced (i.e. uncoupled) rectangular cross-section with a layup of [0/90/0] is discussed, while the

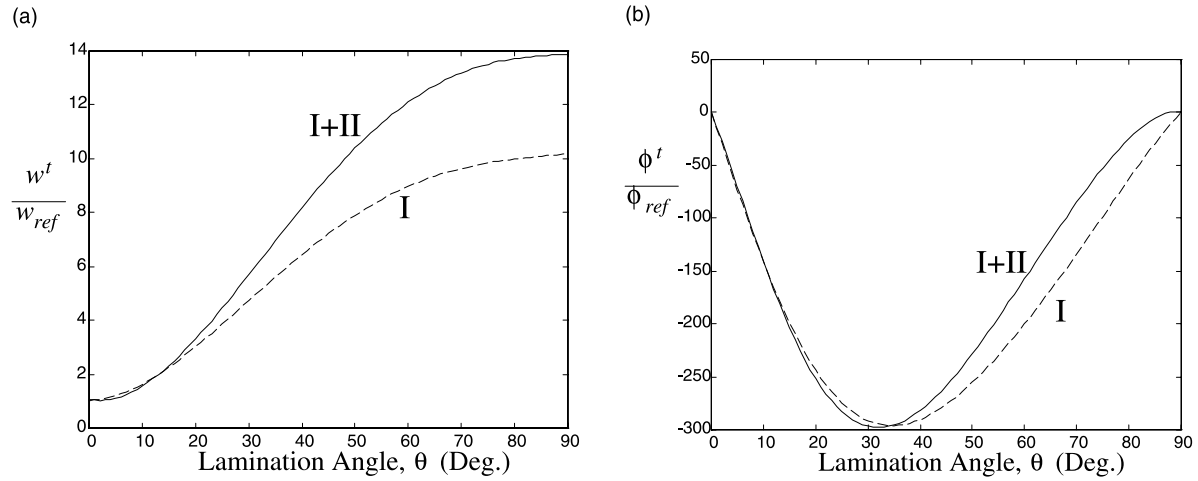

Fig. 7. (a) Tip beamwise displacement. (b) Tip twist angle due to a tip beamwise load: $\phi_{\text{ref}} = (F_z^{\text{t}} l^2)/(3C_{11}(0))I_{zz}$.

clamped-free beam is assumed to undergo a beamwise tip force, F_z^{t}. Clearly, to obtain a complete solution in these case, all three solution levels are required. The rectangular cross-section dimensions $a : b = 2 : 1$ are shown in Fig. 8, where an illustrative cross-sectional discretization is shown. The numerical results presented in what follows are for $N = 21$ and $M = 15$.

For the present configuration and loading mode, zero values for the cross-sectional displacements $u(x)$, $v(x)$, and $\phi(x)$ were obtained, while a tip beamwise displacement of $w^{\text{t}}/w_{\text{ref}} = 1.09$ (where $w_{\text{ref}} = (F_z^{\text{t}} l^3)/(3C_{11}(0)I_{zz})$) has been reached.

The following discussion will describe the above composite beam behavior in more details by comparing the results with the case where only solution levels I and II are used. The three warping components are presented in Fig. 9a–c. The out-of-plane warping Ψ^u shown in Fig. 9a exhibits linear variation over the 90°

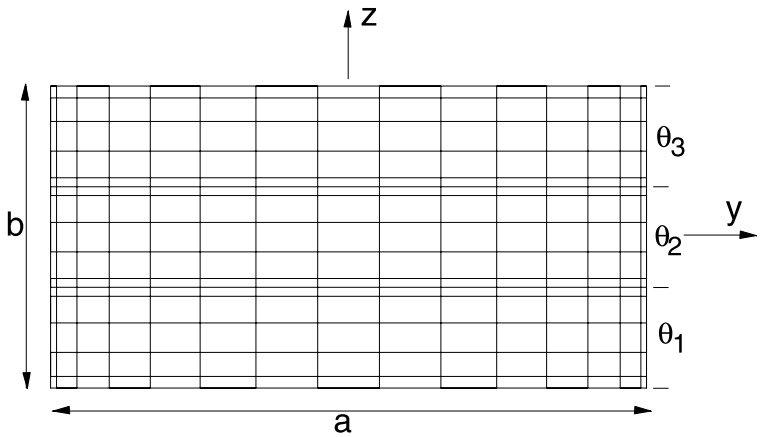

Fig. 8. Undeformed discretized rectangular cross-section applied for three laminae. The finite-difference solution is based on a meshing scheme which is refined towards the lamina free surfaces or interlaminar lines (using a "cosine rule"). Layup notation is $[\theta_1, \theta_2, \theta_3]$.

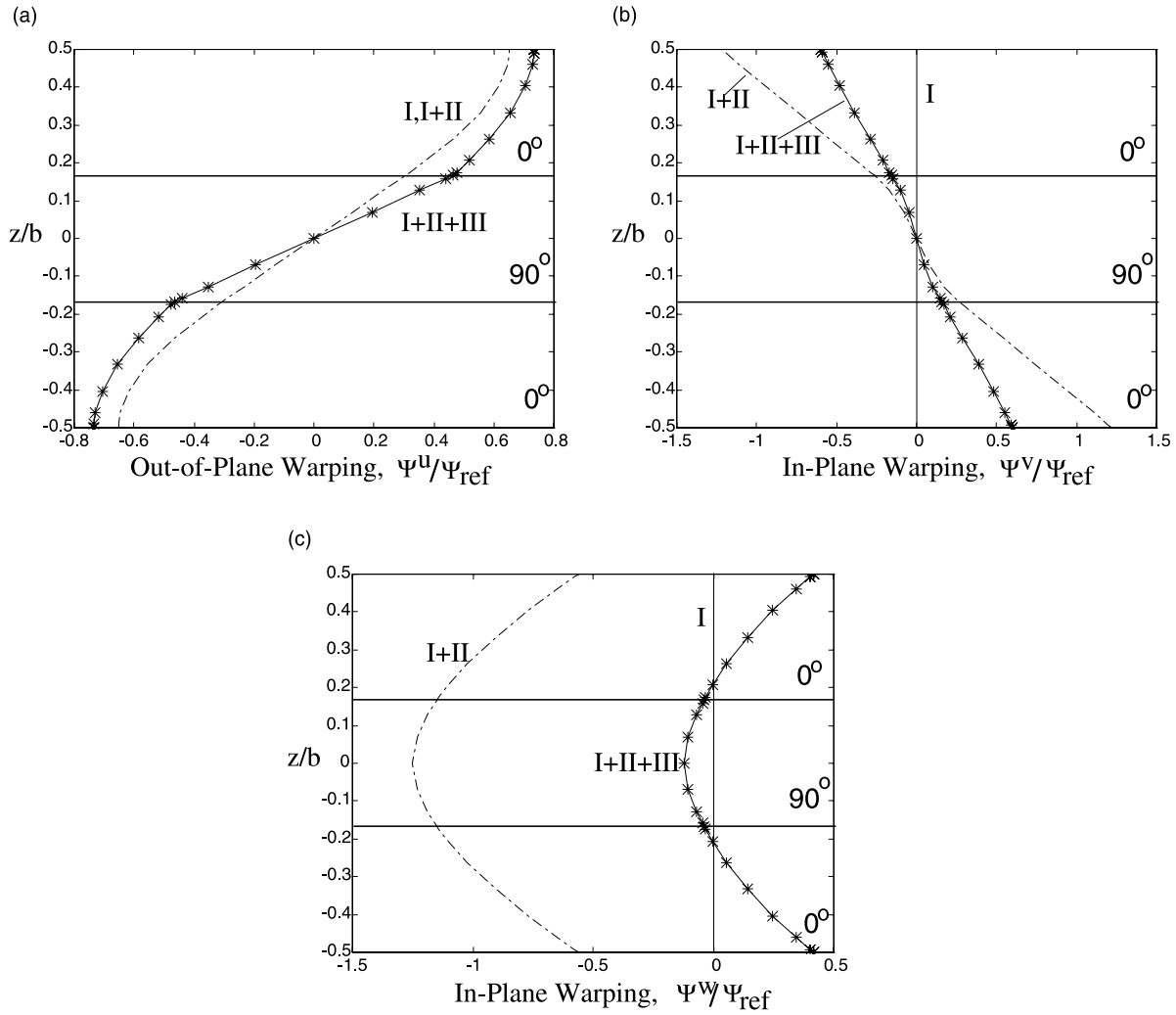

Fig. 9. (a) The distribution of the out-of-plane warping, Ψ^u. (b) The distribution of the in-plane warping, Ψ^v. (c) The distribution of the in-plane warping, Ψ^w, due to a beamwise tip load over a rectangular cross-section. $\Psi_{\text{ref}} = aC_{66}(0)/F_z^{\text{t}}$, $x/L = 0.5$, $y/a = -0.3$. The (*) symbols indicate the finite-difference control points.

lamina and different higher order variation over the 0° laminae. It is also demonstrated that in order to maintain a continuous stress distribution, the warping on both sides of the interface lines exhibits different derivatives (with respect to z). As far as the in-plane warping components are concerned, Fig. 9b and c shows that solutions of level I and II only, lead to relatively large discrepancies compared with the complete solution (i.e. I + II + III). Note that no in-plane warping is included in solution level I. These discrepancies are clearer in Fig. 10 where the deformed cross-section is shown. Of special interest is the variation in the deformation along the vertical edges.

The normal and shear stresses are presented in Figs. 11a–c and 12a–c, respectively, while the broken lines represent values that were obtained by solutions levels I and II only. The axial stress σ_{xx} is presented in Fig. 11a. As shown, this stress exhibits a discontinuous distribution and the bending moment is mainly

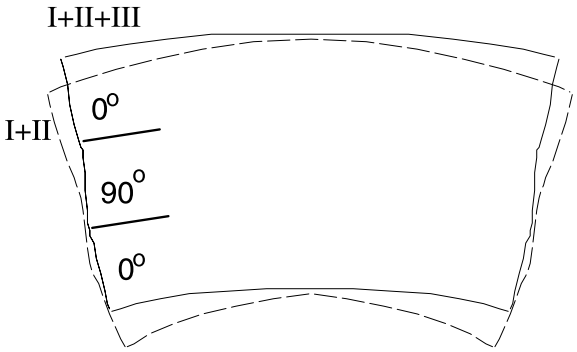

Fig. 10. The deformed cross-section of a clamped-free beam of a rectangular cross-section at $x/L = 0.5$ due to a beamwise tip load $(F_z L^2/(3C_{11}(0)I_{zz}) = 0.0239)$. Note that the solution in level I contains no in-plane warping. The warping magnitude has been multiplied by 1000.

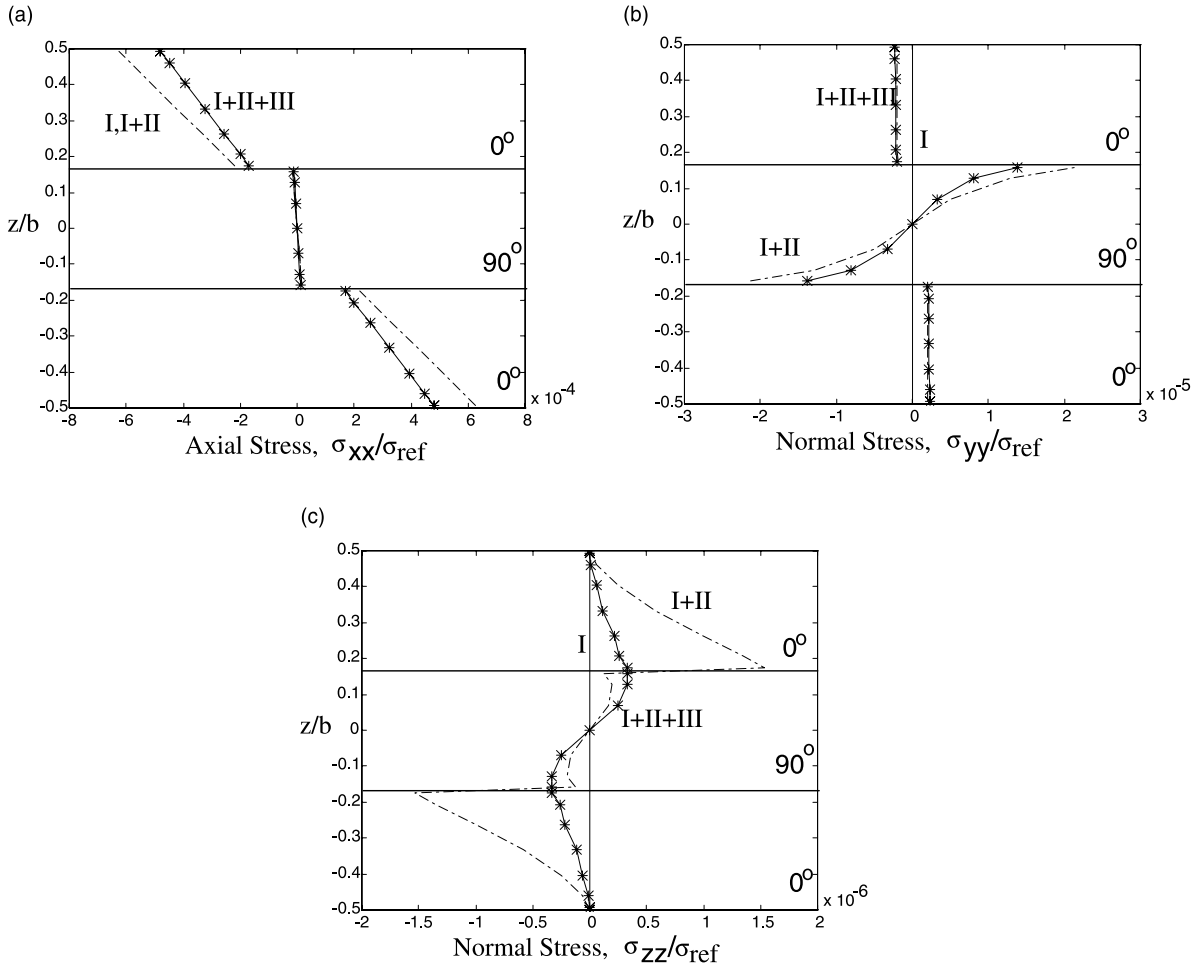

Fig. 11. (a) The distribution of the axial stress, σ_{xx}. (b) The distribution of the normal stress, σ_{yy}. (c) The distribution of the normal stress, σ_{zz}, due to a beamwise tip load over a rectangular cross-section. $\sigma_{\text{ref}} = C_{11}(0)$, $x/L = 0.5$, $y/a = -0.3$. The (*) symbols indicate the finite-difference control points.

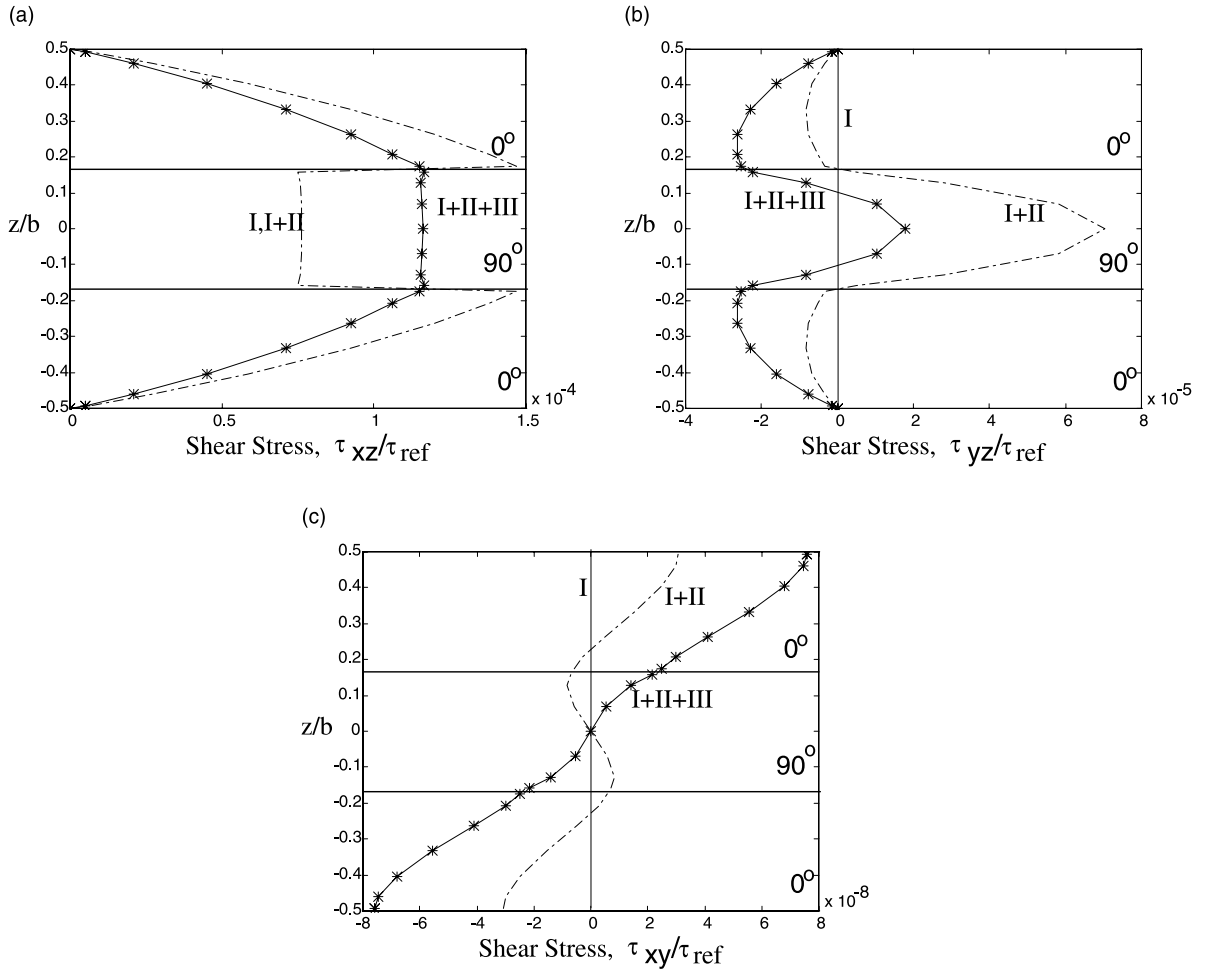

Fig. 12. (a) The distribution of the shear stress, τ_{xz}. (b) The distribution of the shear stress, τ_{yz}. (c) The distribution of the shear stress, τ_{xy}, due to a beamwise tip load over a rectangular cross-section. $\sigma_{\text{ref}} = C_{66}(0)$, $x/L = 0.5$, $y/a = -0.3$. The (*) symbols indicate the finite-difference control points.

supported by the outer laminae. The normal stress σ_{yy} is shown in Fig. 11b from which the compression in the upper lamina and the extension in the lower lamina are clear. The middle lamina is subjected to an alternating σ_{yy} sign. This distribution correlates well with the deformation along the vertical edges shown in Fig. 10. The normal stress σ_{zz} is shown in Fig. 11c which demonstrates that the analysis provided by solution level III is essential for predicting this interlaminar normal stresses. As shown, without the interlaminar analysis provided by level III solution, an error of more than 200% is obtained in the prediction of the interlaminar normal stresses, in addition to a discontinuous distribution.

The shear stress τ_{xz} is presented in Fig. 12a. As shown, this stress is highly influenced by level III solution. In this case, level III solution establishes continuous distribution for this stress and provides an adequate value to the interlaminar values. Similar conclusion is reached for the τ_{yz} component presented in Fig. 12b. The τ_{xy} shown in Fig. 12c is relatively small and plays no role in the present case.

6.2.2. A beam with a "bending-twist" coupling

The discussion will now be focused on the case of and unbalanced beam of a rectangular cross-section with a layup of [30/0/30]. The clamped-free beam undergoes a beamwise tip moment, M_y. The rectangular cross-section dimensions and discretization are identical to those reported for the previous example.

The above unbalanced symmetric layup induce a beamwise bending-torsion coupling. Subsequently a tip beamwise deflection of $w^t/w_{ref} = 1.71$ and a tip twist of a $\phi^t/\phi_{ref} = 2.09$ (where $\phi_{ref} = \left(F_z^t l^2\right)/(3C_{11}(0)I_{zz})$) have been obtained.

The distribution of the interlaminar shear stresses τ_{xz} is presented in Fig. 13. As shown, a dramatic increase of this stress occurs along the vertical edges and in the vicinity of the interlaminar lines. This observation matches the findings observed in Wang and Choi (1982) where analysis which is focused on the boundary-layer effects is reported. Note that the net F_z resultant force vanishes in this case.

The distribution of the τ_{xy} shear stresses is presented in Fig. 14. Since this distribution is not continuous across the interlaminar lines, separate distributions for the three laminae are presented. Again, sharp increase of this stress is observed in the vicinity of the interlaminar lines.

7. Concluding remarks

A solution methodology based on a multilevel analysis of laminated composite beam has been devised. The analysis employs a simple iterative procedure which carries out a series of solutions, while each solution is responsible for introducing a different level of physical phenomena. The solution hierarchy has been designed in such a way that each level is focused on a different set of unknowns. This hierarchy ensures that the results of lower levels are considered as a nearly constant background state for the higher level analyses, while the results of higher levels may be considered as having a secondary or small effect on the lower level results. The paper summarizes the proposed solution strategy and its implementation for generic cases using a finite-difference based scheme.

Overall, the solution provides a three-dimensional solution for composite beam behavior due to a generic load distribution that may handle all levels of deformation which are usually differ by orders of

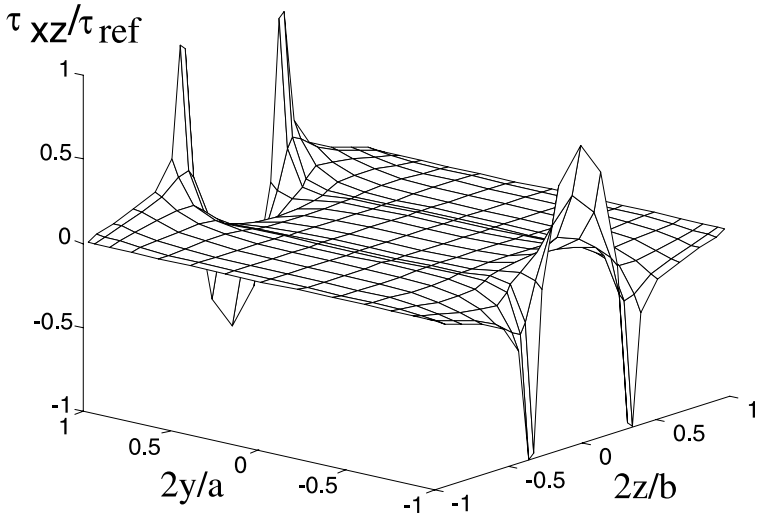

Fig. 13. The distribution of the shear stress, τ_{xz}, due to a beamwise tip load over a rectangular cross-section ($\tau_{ref} = \tau_{xz}(\max)$, $x/L = 0.5$).

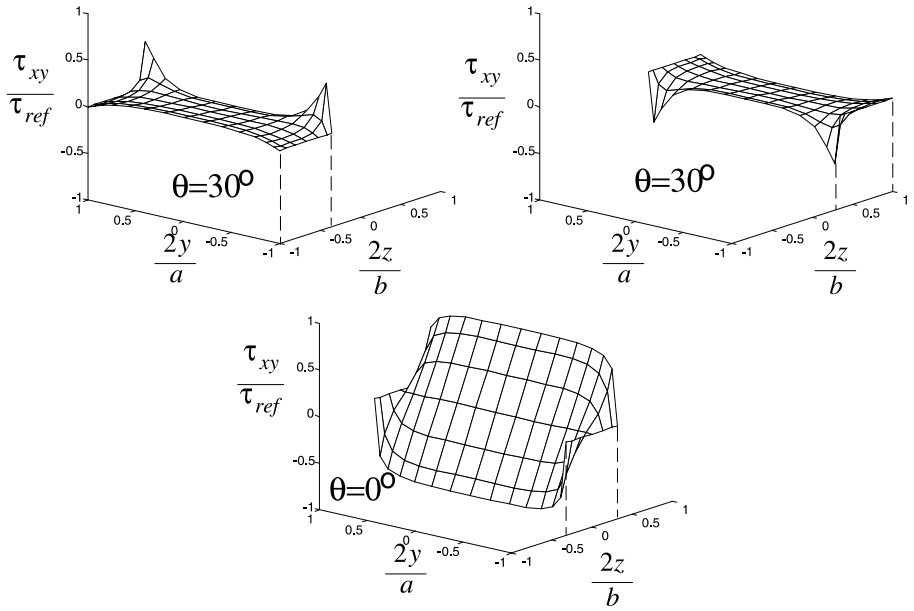

Fig. 14. The distribution of the shear stress, τ_{xy}, due to a beamwise tip load over a rectangular cross-section ($\tau_{\text{ref}} = \tau_{xy}(\max)$, $x/L = 0.5$).

magnitude. Starting from the global beam deformation, the solution includes all warping components and interlaminar effects, and supplies an insight into the main physical phenomena at each level.

It should be emphasized that the present methodology is independent and decoupled from any numerical methodology. The closed form analytic solution for a simple configuration which is offered in this paper testifies to this fact.

References

Belsky, M., Beall, M.W., Fish, J., Shephard, M.S., Gomaa, S., 1995. Computer-aided multiscale modelling tools for composite materials and structures. Computing Systems in Engineering 6 (3), 213–223.

Berdichevsky, V., Armanios, E., Badir, A., 1992. Theory of anisotropic thin-walled closed-cross-section beams. Composites Engineering 2 (5–7), 411–432.

Bull, J.W. (Ed.), 1995. Numerical analysis and modelling of composite materials, Analysis of composite rotor blades. Chapman & Hall, London (Chapter 1).

Chandra, R., Stemple, A.D., Chopra, I., 1990. Thin-walled composite beams under bending, torsional, and extensional loads. Journal of Aircraft 27 (7), 619–625.

Chandrashekhara, K., Bangera, K.M., 1992. Free vibration of composite beams using a refined shear flexible beam element. Computers and Structures 43 (4), 719–727.

Chen, W.-H., Huang, T.-F., 1997. Stress singularity of edge delamination in angle-ply and cross-ply laminates. Journal of Applied Mechanics 64, 525–531.

Fish, J., Markolefas, S., 1994. Adaptive global–local refinement strategy based on the interior error estimates of the *h*-method. International Journal for Numerical Methods in Engineering 37, 827–838.

Giavotto, V., Borri, M., Mantegazza, P., Ghiringhelli, G., Carmaschi, V., Maffioli, G.C., Mussi, F., 1983. Anisotropic beam theory and applications. Computers and Structures 16, 402–413.

Kapania, R.K., Raciti, S., 1989. Recent advances in analysis of laminated beams and plates, part I: shear effects and buckling. AIAA Journal 27 (7), 923–934.

Maiti, D.K., Sinha, P.K., 1994. Bending and free vibration analysis of shear deformable laminated composite beams by finite element methods. Journal of Composite Materials 29 (1), 421–431.

Mitchell, J.A., Reddy, J.N., 1998. A multilevel hierarchical preconditioner for thin elastic solids. International Journal for Numerical Methods in Engineering 43, 1383–1400.

Noor, A.K., Burton, W.S., 1989. Assessment of shear deformation theories for multilayered composite plates. Appl. Mech. Rev. 42 (1), 1–12.

Nosier, A., Reddy, J.N., 1992. On vibration and buckling of symmetric laminated plates according to shear deformation theories. Acta Mechanica 94, 123–169.

Ochoa, O.O., Reddy, J.N., 1992. Finite Element Analysis of Composite Laminates. Kluwer, The Netherlands.

Rand, O., 1994. Nonlinear analysis of orthotropic beams of solid cross-sections. Journal of Composite Structures 29 (1), 27–45.

Rand, O., Barkai, S.M., 1996. Analytic insight into the structural couplings and nonlinear formulation of solid and thin-walled composite blades. 52nd Annual Forum of the American Helicopter Society 2, 927–941.

Reddy, J.N., 1989. On refined computational models of composite laminates. International Journal for Numerical Methods in Engineering 27, 361–382.

Reddy, J.N., 1990. A review of refined theories of laminated composite plates. Shock Vibrations Digest 22, 3–17.

Robbins, D.H., Reddy, J.N., 1993. Modelling of thick composites using a layerwise laminate theory. International Journal for Numerical Methods in Engineering 36, 655–677.

Savoia, M., Laudiero, F., Tralli, A., 1993a. A refined theory for laminated beams: part I. New high order approach. Meccanica 28 (October), 39–51.

Savoia, M., Laudiero, F., Tralli, A., 1993b. A refined theory for laminated beams: part II. An iterative variational approach. Meccanica 28 (October), 217–255.

Smith, E.C., Chopra, I., 1993. Air and ground resonance of helicopters with elastically tailored composite rotor. Journal of the American Helicopter Society 38 (4), 50–61.

Stemple, A.D., Lee, S.W., 1989 (April). Large Deflection Static and Dynamic Finite Element Analysis of Composite Beams with Arbitrary Cross-Sectional Warping. 30th AIAA/ASME/ASCE/AHS Structures, Structural Dynamics and Materials Conference. AIAA Paper 89-1363-CP, pp. 1789–1798.

Tracy, A.L., Chopra, I., 1995. Aeroelastic analysis of a composite bearingless rotor in forward flight using an improved warping model. Journal of the American Helicopter Society 40 (3), 80–91.

Wang, S.S., Choi, I., 1982. Boundary-layer effect in composite laminates: part 1. Free-edge stress singularities. Journal of Applied Mechanics 49 (September), 541–548.

Yamane, T., Friedmann, P.P., 1993. Aeroelastic tailoring analysis for preliminary design of advanced propellers with composite blades. Journal of Aircraft 30 (1), 119–126.